

EFFECT OF SOIL ARCHING ON LATERAL SOIL PRESSURES ACTING UPON
RIGID RETAINING WALLS

A THESIS SUBMITTED TO
THE GRADUATE SCHOOL OF NATURAL AND APPLIED SCIENCES
OF
MIDDLE EAST TECHNICAL UNIVERSITY

BY

NIHAN AYDIN ERTUĞRUL

IN PARTIAL FULFILLMENT OF THE REQUIREMENTS
FOR
THE DEGREE OF MASTER OF SCIENCE
IN
CIVIL ENGINEERING

JUNE, 2013

Approval of the thesis:

**EFFECT OF SOIL ARCHING ON LATERAL SOIL PRESSURES ACTING UPON
RIGID RETAINING WALLS**

submitted by **NİHAN AYDIN ERTUĞRUL** in partial fulfillment of the requirements for
the degree of **Master of Science in Civil Engineering Department, Middle East
Technical University** by,

Prof. Dr. Canan ÖZGEN
Dean, Graduate School of **Natural and Applied Sciences**

Prof. Dr. Ahmet Cevdet YALÇINER
Head of Department, **Civil Engineering**

Prof. Dr. Erdal ÇOKÇA
Supervisor, **Civil Engineering Dept., METU**

Prof. Dr. Yener ÖZKAN
Co-supervisor, **Civil Engineering Dept., METU**

Examining Committee Members:

Prof. Dr. M. Ufuk ERGUN
Civil Engineering Dept., METU

Prof. Dr. Erdal ÇOKÇA
Civil Engineering Dept., METU

Prof. Dr. M. Yener ÖZKAN
Civil Engineering Dept., METU

Prof. Dr. Tamer TOPAL
Geological Engineering Dept., METU

Inst. Dr. N. Kartal TOKER
Civil Engineering Dept., METU

Date:

19/06/2013

I hereby declare that all information in this document has been obtained and presented in accordance with academic rules and ethical conduct. I also declare that, as required by these rules and conduct, I have fully cited and referenced all material and results that are not original to this work.

Name, Last name : Nihan AYDIN ERTUĞRUL

Signature :

ABSTRACT

EFFECT OF SOIL ARCHING ON LATERAL EARTH PRESSURES ACTING UPON RIGID RETAINING WALLS

AYDIN ERTUĞRUL, Nihan

M.Sc., Department of Civil Engineering

Supervisor: Prof. Dr. Erdal ÇOKÇA

Co-Supervisor: Prof. Dr. M. Yener ÖZKAN

June 2013, 61 pages

Retaining walls are encountered in various fields of civil engineering. In many practical applications, the earth pressure against rigid retaining walls are calculated using either Coulomb's or Rankine's lateral earth pressure theories. For the sake of simplicity, it is assumed that the lateral earth pressure distribution is linear; however, many experimental results indicated it is significantly nonlinear. Previous physical modeling studies indicated that this nonlinearity results from arching behavior induced within the granular backfill. In this study, lateral active earth pressures acting on yielding rigid retaining walls are studied by considering arching effects. Previous lateral earth pressure theories that take into account of soil arching are modified. For this purpose, new analytical formulations considering arching effects are suggested to predict lateral active earth pressures. In these proposed methodologies, shape of the failure surface and soil arch geometries are changed for better representation of the actual behavior. Additionally, effect of surcharge on lateral earth pressures is discussed. Pressure distributions estimated by the proposed methodologies were validated against physical test data and compared with the previous theories. Parametric studies indicate that active earth pressure distributions change from triangular to curvilinear as the effect of soil arching increases. Wall backfill interface friction is found as the main factor influencing the arching effect. Lateral soil pressures calculated according to parabolic failure line assumption provide better agreement with the actual test results. Application point of the total thrust rises up to $0.43H$ which is approximately 30% higher than the mostly used value of $0.33H$.

Keywords: Arching Effect, Lateral Earth Pressure, Parabolic Failure Surface, Surcharge Load

ÖZ

KEMERLENME DAVRANIŞININ RİJİT İSTİNAT DUVARLARINA ETKİ EDEN YANAL ZEMİN BASINÇLARI ÜZERİNDEKİ ETKİSİ

AYDIN ERTUĞRUL, Nihan

Yüksek Lisans, İnşaat Mühendisliği Bölümü

Tez Yöneticisi: Prof. Dr. Erdal ÇOKÇA

Ortak Tez Yöneticisi: Prof. Dr. M. Yener ÖZKAN

Haziran 2013, 61 sayfa

Çeşitli inşaat mühendisliği uygulamalarında istinat duvarlarıyla sıkça karşılaşmaktadır. Pratikte, rijit istinat duvarlarına etkiyen yatay zemin basınçları Coulomb ya da Rankine yatay zemin basıncı teorileriyle tahmin edilmektedir. Kolay bir çözüm için, yatay zemin basıncının doğrusal olarak arttığı kabul edilmektedir; ancak yapılan pek çok deneysel çalışmada, yüzeyi sürtünmeli istinat yapılarına etkiyen basınç dağılımlarının belirgin biçimde eğrisel formda olduğu görülmüştür. Deneysel çalışmalar eğriselliğin granüler art dolgu bünyesinde oluşan kemerlenme etkisinden kaynaklandığını ortaya koymaktadır. Bu çalışmada, yatay ötelenme yapabilen rijit istinat duvarlarına etkiyen yatay zemin basınçları, kemerlenme etkileri dikkate alınarak incelenmektedir. Önceki teoriler zemin davranışının daha gerçekçi bir şekilde modellenebilmesi için kemerlenme etkisi göz önüne alınarak yeniden değerlendirilmektedir. Bu amaçla yatay basınçlar için yeni analitik formülasyonlar sunulmaktadır. Art dolgu içerisindeki kayma düzleminin şekli ve kemer geometrileri değiştirilerek gerçek davranışın daha iyi modellenebilmesi hedeflenmiştir. Sürşarj yükü etkisiyle oluşan yatay zemin basınçları da kemerlenme teorisi ışığında irdelenmiştir. Önerilen formülasyonlar, fiziksel deney bulguları ve diğer teorilerle karşılaştırılarak doğrulanmaya çalışılmıştır. Parametrik çalışmalar, basınç dağılımlarının lineer formdan eğrisel bir hal aldığı göstermektedir. Duvar art dolgu sürtünmesinin, kemerlenmeyi değiştiren en önemli parametre olduğu görülmüştür. Parabolik kemerlenme dikkate alınarak geliştirilen formülasyonlar, deney verileriyle daha iyi örtüşme sağlamıştır. Basınç dağılımındaki eğrisellik, artan kemerlenme etkisiyle daha belirginleşmekte ve toplam itkinin uygulama noktası yaklaşık olarak 0.43H seviyelerine çıkarak yaygın olarak kabul edilen 0.33H değerinden %30 daha yukarıda oluşmaktadır.

Anahtar Kelimeler: Kemerlenme Etkisi, Parabolik Kayma Yüzeyi, Sürşarj Yükü, Yatay Zemin Basıncı

ACKNOWLEDGEMENTS

I wish to express my appreciation to my supervisor Prof. Dr. Erdal OKA and my co-supervisor Prof. Dr. M. Yener ZKAN for their guidance, encouragement, positive attitude throughout the whole phases of the research and valuable insight throughout this research. Their wise attitude enlightened me in all stages of my graduate studies. Without their valuable support, the completion of this study would be nearly impossible.

Finally, I would like to express the most grateful thanks to my husband zgür Lutfi ERTUĐRUL for his encouragement, insightful comments and to my family, for their continuous patience and support. I would like to extend my appreciation to Gzde BİLGİN for her support.

TO MY TWIN SONS

TABLE OF CONTENTS

ABSTRACT.....	iv
ÖZ.....	v
ACKNOWLEDGEMENTS.....	vi
TABLE OF CONTENTS.....	viii
LIST OF TABLES.....	x
LIST OF FIGURES.....	xi
LIST OF SYMBOLS.....	xiii
CHAPTERS	
1 INTRODUCTION.....	1
1.1 General.....	1
1.2 Scope of the Study.....	1
2 LITERATURE REVIEW.....	3
2.1 Introduction.....	3
2.2 Theories of Lateral Earth Pressure.....	3
2.3 Previous studies on the earth-retaining walls.....	6
2.4 Previous Studies Related to Soil Arching.....	6
2.5 Analytical Modeling Studies on Soil Arching.....	7
2.6 Numerical Modeling Studies on Soil Arching.....	8
2.7 Physical Modeling Studies on Soil Arching.....	11
2.8 Analytical Studies on the Soil Arching Behavior.....	11
2.9 Surcharge Induced Pressures Behind Retaining Walls.....	18
3 ANALYTICAL MODELING OF SOIL ARCHING.....	21
3.1 Introduction.....	21
3.2 Lateral Earth Pressure Distribution Considering Planar Failure Surface and Circular Soil Arch Formation within the Failure Zone.....	22
3.3 Modification of Paik and Salgado Lateral Soil Arching (2003) Approach Assuming Planar Failure Surface and Parabolic Soil Arch within the Backfill (<i>Method I</i>).....	22
3.3.1 Determination of the Rotation angle, θ	26
3.3.2 Determination of lateral soil pressure acting on retaining wall.....	28
3.4 Modification of Paik and Salgado Lateral Soil Arching (2003) Approach Assuming Curvilinear Failure Surface and Circular Soil Arch in Backfill (<i>Method II</i>).....	30
3.4.1 Parabolic failure surface with Spangler-Handy's boundary conditions.....	30
3.5 Modification of Paik and Salgado Lateral Soil Arching (2003) Approach to Include Surcharge Effect on the Lateral Earth Pressure Distribution.....	33
4 PARAMETRIC STUDY.....	35
4.1 Introduction.....	35
4.2 Parametric Analyses Regarding the Distribution of Lateral Active Soil Pressures.....	35

4.2.1	Lateral Active Soil Pressures.....	35
4.2.2	Effect of internal friction angle on lateral active earth pressures	39
4.2.3	Effect of wall-backfill interface friction angle on lateral active earth pressures	40
4.2.4	Effect of retaining wall height on lateral active earth pressures.....	43
4.3	Comparison of Lateral Active Earth Thrust Calculated with Different Methods	44
4.3.1	Comparison of lateral active earth thrust normalized with Coulomb’s total lateral active earth thrust	45
4.3.2	Effect of internal friction angle on lateral active earth thrust.....	45
4.3.3	Effect of wall-backfill interface friction angle on lateral active earth thrust.. ..	46
4.4	Application Point of the Total Lateral Active Thrust	47
4.4.1	Height of application point of lateral active earth force normalized with wall height.....	47
4.4.2	Effect of internal friction angle on the point of application of lateral active force.....	48
4.4.3	Effect of wall-backfill interface friction angle on the point of application of lateral active force	49
4.5	Comparison of Lateral Earth Pressure Coefficients Calculated with the Suggested Formulations	50
5.	SUMMARY AND CONCLUSION	53
5.1	Summary.....	53
5.2	Research Findings.....	53
5.3	Conclusions	55
5.4	Recommendations for Future Work	56
	REFERENCES.....	57
	APPENDIX A	59
A.	DERIVATION	59
A.1	Determination of the Rotation Angle	59
A.2	Determination of the Rate of Change of Failure Angle.....	59
A.3	Determination of Paik and Salgado Lateral Arching (2003) Approach to Include Surcharge Effect.....	60

LIST OF TABLES

TABLES

Table 2-1 Effect of surcharge location on the retaining structure (AASHTO, 1987).....	19
Table 4-1 Total lateral active earth force normalized with Coulomb's total lateral earth thrust	45
Table 4-2 Height of application point of lateral active earth force normalized with wall height	48

LIST OF FIGURES

FIGURES

Figure 2-1 Graphical depictions of (a) Coulomb's lateral active earth pressure theory (1776) (b) Rankine's lateral active soil pressure theory (1857)	4
Figure 2-2 Active and passive conditions for translating rigid retaining walls.....	4
Figure 2-3 Possible displacement modes of an L-shaped retaining wall: (a) structural flexure, (b) base rotation, (c) base translation, and (d) sliding (Gazetas, et al., 2004).....	5
Figure 2-4 An illustration of wall backfill interface.....	6
Figure 2-5 Stress redistribution in granular soil due to downward movement of a long narrow trapdoor resulting in soil arching (Terzaghi, 1943).....	8
Figure 2-6 Soil arching mechanism in soft soil supported by stone column (Deb, 2010) ...	8
Figure 2-7 Displacement field of granular soil on the trap-door numerical modeling for $\delta=19$ mm (Chevalier et al., 2008)	9
Figure 2-8 Discrete element modeling of (a) prismatic sand heap, (b) force chains (Nadukuru and Michalowski, 2012).....	10
Figure 2-9 Displacements due to wall rotation of 0.008 radian about the top edge (Nadukuru and Michalowski, 2012).....	10
Figure 2-10 Arching phenomena interpreted schematically for the wall rotation about top (Nadukuru and Michalowski, 2012).....	11
Figure 2-11 Observed failure mechanism in the granular soil for different relative displacements (δ/B) (Costa et al., 2009).....	11
Figure 2-12 (a) Mohr circle representation of stresses due to soil arching close to the rough wall, (b) continuous inverted arch described as trajectory of minor principal stresses inside the vertical walled trench according to Krynine Approach (Handy, 1985).....	13
Figure 2-13 The graphical representation of lateral soil arching indicating the formation of catenary minor arches and shear lines for active stress conditions against a retaining wall (Handy, 1985).....	14
Figure 2-14 Forces acting on an infinitesimal element taken from the wedge (Wang, 2000)	15
Figure 2-15 Trajectory of minor principal stresses of the cohesionless material in trench (Paik and Salgado, 2003).....	17
Figure 2-16 Comparison of measured and predicted active earth pressure distributions (Paik and Salgado, 2003).....	18
Figure 2-17 Effect of surcharge on retaining walls (AASHTO,1987)	18
Figure 3-1 Rigid retaining wall that translates horizontally away from the soil	22
Figure 3-2 Directions of the major and minor principal stresses on the differential parabolic element in the granular backfill behind rigid retaining wall	23
Figure 3-3 Trigonometric relations at point A to obtain active lateral stress ratio, σ_{ahw} , on wall.....	24
Figure 3-4 Horizontal and vertical stresses on the differential flat element within in the granular backfill	25

Figure 3-5 Mohr circle to determine the rotation angle, θ	26
Figure 3-6 Free body diagram of differential flat element with planar failure surface for Method I.....	29
Figure 3-7 Schematic representation of two different failure surfaces (a) parabolic (b) planar failure surface.....	30
Figure 3-8 Parabolic failure surface with Spangler-Handy Boundary Conditions	31
Figure 3-9 Graphical depiction of horizontal slices within parabolic failure surface with Spangler and Handy's (1984) boundary conditions.....	32
Figure 4-1 Comparison of lateral active earth pressure distributions predicted with different methods and physical test results.....	36
Figure 4-2 Comparison of lateral active earth pressure distributions predicted with different methods with the physical test results (Data of Tsagarelli,1965 and Rankine's theory are removed from the previous figure).	37
Figure 4-3 Comparison of surcharge induced lateral active earth pressures for different approaches	38
Figure 4-4 Lateral active earth pressure distributions obtained by Method I and Method II for various ϕ values.....	39
Figure 4-5 Lateral active earth pressure distributions under surcharge load of $q=\gamma H$ for various backfill internal friction angles (ϕ).....	40
Figure 4-6 Lateral active earth pressure distribution for various wall-backfill interface friction angles (δ).....	42
Figure 4-7 Lateral active earth pressure distributions under surcharge load of $q=\gamma H$ for various wall-backfill interface friction angles (δ).....	43
Figure 4-8 Effect of earth pressure distribution with the height of retaining wall.....	44
Figure 4-9 Effect of internal friction angle on lateral active force	46
Figure 4-10 Effect of wall-backfill interface friction angle on lateral active earth force ..	47
Figure 4-11 Effect of backfill internal friction angle on normalized height of application of lateral active earth force.....	49
Figure 4-12 Effect of δ on the height of application of lateral active earth force.....	50
Figure 4-13 Effect of ϕ and δ lateral active earth pressure coefficients for granular soils	51
Figure 7-1 A slice showing the failure angle within the failure zone at the back of the retaining wall	52

LIST OF SYMBOLS

A	ratio of the width of failure plane at ground level for parabolic failure surface to the width of failure plane at ground level for planar failure surface
B	width of the trench
B_z	width of any differential flat element at depth z
C	integral constant
d_z	thickness of differential flat element
h	height of the application point of total lateral active earth thrust from the base of the wall
H	retaining wall height
K_w	active lateral earth pressure ratio for circle arch suggested by Handy (1985)
K_a	coefficient of active lateral earth pressure
K_0	lateral earth pressure coefficient given by Jaky (1944)
K_{ap}	active lateral earth pressure ratio for parabolic concave arch
K_{awn}	active lateral earth pressure ratio for circle arch suggested by Paik and Salgado (2003)
K_q	surcharge coefficient proposed by Wang (2000)
K_γ	backfill coefficient proposed by Wang (2000)
N	ratio of major principal stress to minor principal stress
q	surcharge
R	radius of minor principal stress trajectory
x	horizontal distance from retaining wall
z	depth of retaining wall from the surface of backfill
α	angle of failure surface with respect to horizontal
α_i	rate of change of failure angle for the horizontal slice method
β	parameter defining the shape of parabolic arch
γ	total unit weight of the retained soil
φ	internal friction angle of the backfill
θ	angle between tangent to σ_3 trajectory and vertical at the wall
δ	interface friction angle between the wall and backfill
μ	friction coefficient at the interface between wall and backfill, $\tan \delta$
σ_1	major principal stress
σ_3	minor principal stress
σ_{ah}	active lateral stress at an arbitrary point on differential flat element
σ_{ahw}	active lateral stress on retaining wall
σ_{vw}	vertical stress on retaining wall
τ_f	frictional resistance at critical failure surface
τ_w	frictional resistance of the wall
ψ	angle between tangent to σ_3 trajectory and vertical at an arbitrary point

CHAPTER 1

INTRODUCTION

1.1 General

The calculation of lateral earth pressures on soil retaining walls induced by granular backfill and surcharge loads is one of the oldest problems of soil mechanics. Coulomb's (1776) and Rankine's (1857) theories, which are based on limit equilibrium techniques are extensively used to calculate the lateral soil pressures acting on soil retaining walls. Rankine's theory is applicable for the calculation of the earth pressure on vertical, perfectly smooth walls however the interfaces between retaining walls and backfills are far from frictionless. Coulomb's theory was established on the basis of the equilibrium of the forces on a sliding wedge between the plane of failure and the back face of the retaining wall hence it could not estimate the shape of the lateral stress distribution. On the other hand, Rankine assumes a triangular stress distribution of earth pressures against retaining walls. Based on the results of experimental studies (Fang and Ishibashi, 1986), it was observed that pressure distribution against translating and rigid retaining walls are significantly non-linear due to soil arching. Recent studies demonstrated positive role of soil arching on the lateral earth pressure distribution against retaining walls. The horizontal arching mechanism significantly affects horizontal earth force by causing stress distribution within the backfill soil elements via soil shear stresses. Analytical methods which incorporate soil arching to lateral earth pressure theories provide more realistic estimations of the lateral earth stresses (Paik and Salgado, 2003). Calculation of lateral stresses considering soil arching effects may lead to economical and effective design of retaining structures in geotechnical applications. Since soil arching is a very complex phenomenon, utilization of numerical and experimental modeling techniques with analytical approaches may provide useful insight towards understanding this complex problem of soil mechanics.

1.2 Scope of the Study

In this study, a new analytical procedure is proposed to estimate lateral stresses against rigid and yielding walls considering lateral soil arching effect. The limitations of the previous studies and the contribution of the proposed methodology are discussed in detail in the following chapters. The methods described herein concentrates on the lateral earth pressures against rigid walls with a translational mode of movement. The granular backfill material is characterized with its angle of internal friction. The effect of soil internal friction angle and the wall-backfill friction angle is taken into account in the analyses. The distribution of the earth pressure along the retaining wall height is compared to data obtained from previous physical modeling studies and those of previous analytical

approaches. The validated analytical model is further used to carry out parametric analyses to investigate the effect of soil arching for various combinations of backfill attributes.

Based on the results of the current study, simplified charts are proposed for estimating lateral active pressures, lateral thrust and application points for different combinations of backfill friction angle and interface friction parameters.

CHAPTER 2

LITERATURE REVIEW

2.1 Introduction

In this chapter, a brief summary of the studies on the lateral active earth pressures acting on rigid and translating retaining walls are given. Two of the most well-known earth pressure theories, namely Coulomb's and Rankine's Earth Pressure Theories are discussed in this context. Next, results of previous physical modeling studies performed to investigate the lateral soil pressure distribution on the rigid retaining walls are discussed. At the last section of this chapter, the analytical, numerical and physical modeling studies on the lateral soil arching are summarized.

2.2 Theories of Lateral Earth Pressure

There are two commonly accepted theories for calculating lateral earth pressures, namely Coulomb's Lateral Earth Pressure Theory (1776) and Rankine's Earth Pressure Theory (1857). These theories are based on the common assumptions that the retained soil is homogeneous, isotropic, semi-infinite and well drained to avoid consideration of pore pressures. Graphical depiction of the Coulomb's and Rankine's Theories are given in Figure 2-1.

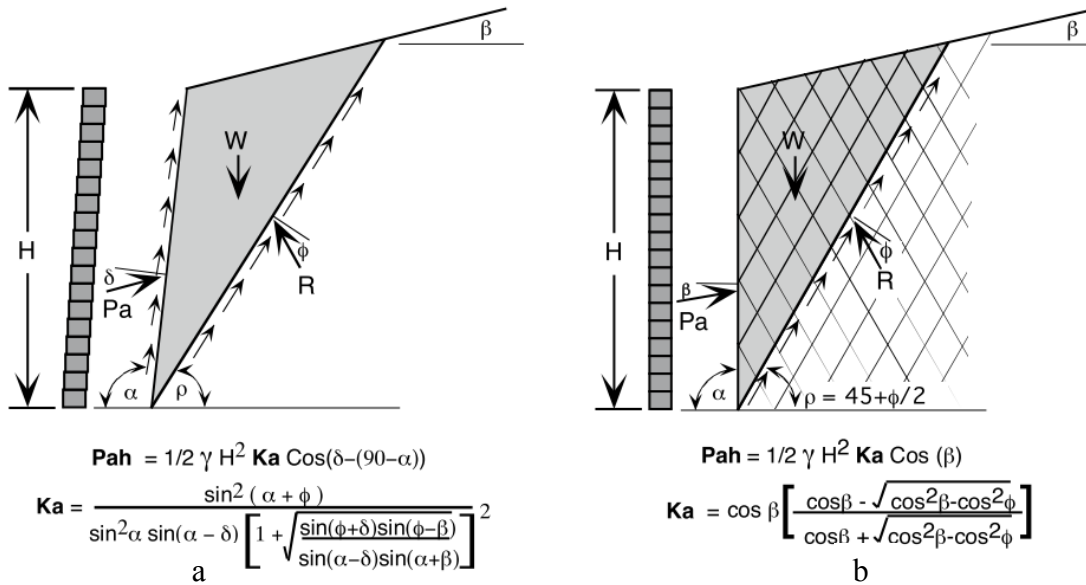


Figure 2-1 Graphical depictions of (a) Coulomb's lateral active earth pressure theory (1776) (b) Rankine's lateral active soil pressure theory (1857)

The theories of lateral earth pressure against retaining walls account for active and passive earth stresses. The active condition, generally resulting in the lowest earth pressures, occurs when the relative movement between the wall and the soil is away from each other. Figure 2-2 shows the active and passive conditions for translating rigid earth retaining walls.

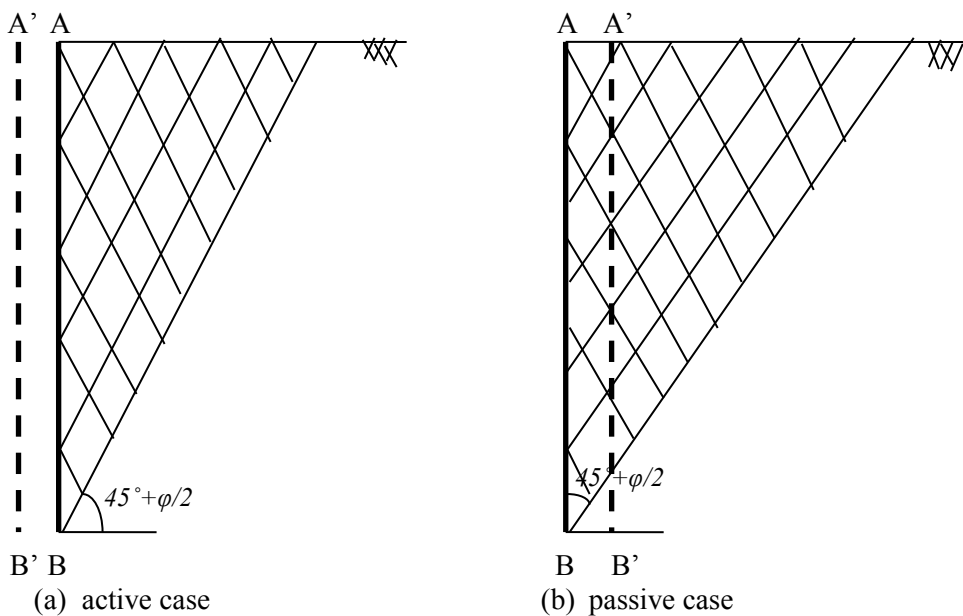


Figure 2-2 Active and passive conditions for translating rigid retaining walls

In order to achieve active state stress conditions within the backfill, retaining wall undergoes flexural deformations, rotational (from the top or base), translational and sliding type displacements. Gazetas et al. (2004) depicted the possible displacement modes of an L-shaped retaining wall in Figure 2-3. The amount of displacement required to reach active state is highly dependent upon the characteristics of the backfill soil and the displacement mode of the retaining wall. Lambe and Whitman (1969) addressed the shear strain requirement necessary to achieve active stress state as very little horizontal strain less than 0.5% of the retaining wall height. The passive condition, resulting in the highest lateral earth pressures, occurs when the wall moves towards the soil mass. In addition to active and passive states of stress, at-rest condition occurs when there is no relative movement between the wall and the soil. Additional pressures can occur due to surcharge or compaction of the retained soil behind the wall.

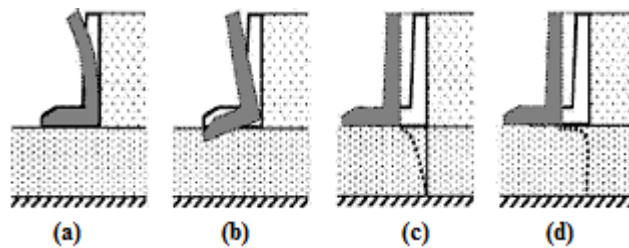


Figure 2-3 Possible displacement modes of an L-shaped retaining wall: (a) structural flexure, (b) base rotation, (c) base translation, and (d) sliding (Gazetas, et al., 2004)

Using identical parameters, the lateral load calculated from Coulomb's theory is less than the earth force calculated by Rankine's theory. It should be noticed that Coulomb's method is a graphical approach considering the equilibrium of the forces acting on the soil wedge and it does not have the ability to give information about the distribution of lateral stress along the wall height. According to Coulomb's theory, a unique failure angle for every design condition exists which is expressed in Equation (2-1) whereas Rankine's theory fixes the internal failure plane at $45^\circ + \varphi/2$.

$$\tan(\rho - \varphi) = \frac{-\tan(\varphi - \beta) + \sqrt{\tan(\varphi - \beta) [\tan(\varphi - \beta) + \cot(\varphi + \iota)] [1 + \tan(\delta - \iota) \cot(\varphi + \iota)]}}{1 + \tan(\delta - \iota) [\tan(\varphi - \beta) + \cot(\varphi + \iota)]} \quad (2-1)$$

where φ is the angle of internal friction angle, ι is the slope of the wall measured from vertical ($\alpha-90$), β is the slope angle above the wall and δ is the angle of friction at the back of the wall.

Additionally, Rankine's theory does not account for the soil-wall interface friction effect. In Figure 2-4 three possible modes of the shear resistance along the wall backfill interface are depicted. In Figure 2-4 (a), smooth wall condition is illustrated. According to this case, retaining wall does not carry any shear stress since there is no wall backfill friction. In Figure 2-4 (b), a rough wall condition is depicted. According to this condition, frictional forces occur along the wall-backfill interface along which shear stress can be carried within the retained material by enabling lateral arching. In Figure 2-4 (c), very rough wall surface is depicted. This type of surface significantly increases the wall-backfill interface friction.

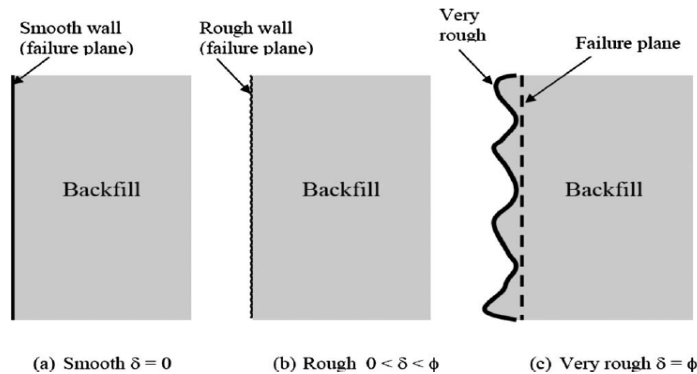


Figure 2-4 An illustration of wall backfill interface

2.3 Previous studies on the earth-retaining walls

Retaining walls are encountered in various fields of civil engineering such as highway and railway projects, hydraulic structures, mining fortifications, etc. Backfill or the retained soil exerts a lateral earth pressure on the retaining wall structure which determines the design of the structure to be built for soil retention. Retaining walls are mainly classified as gravity, semi-gravity, non-gravity and anchored retaining structures. Gravity walls derive their capacity through self weight of the wall and resists overturning and sliding forces of the retained backfill. The gravity wall types include rigid gravity walls and mechanically stabilized earth walls. Semi-gravity walls provide resistance by their structural components to mobilize the dead weight of backfill through cantilever action. Non-gravity retaining walls provide resistance through embedment of vertical wall and interface elements. Anchored walls are similar to non-gravity walls except that they derive their additional capacity to lateral loads by tiers of ground anchors. Anchors are the strands or bars extending from the retaining wall face to soil zone.

Retaining walls can be classified according to the mobilized soil displacements as yielding and non-yielding walls. Yielding walls may have the ability to displace due to earth forces i.e. the wall may deform, translate and rotate. Non-yielding walls such as basement walls, propped walls do not enable horizontal structural deformations due to the lateral earth pressures. Therefore, earth pressures behind the non-yielding retaining walls are greater than these of the active case.

2.4 Previous Studies Related to Soil Arching

Terzaghi (1943) described soil arching as “one of the most universal phenomena encountered in soils both in field and in the laboratory”. Arching effect is encountered in many geotechnical problems such as conduits covered with an embankment, backfilled trenches overlying conduits and backfills behind retaining walls. Studies related to soil arching starts with the classical arching theories of Terzaghi (1943), further extends to several analytical, numerical approaches and physical modeling studies. Arching of the granular materials was first recognized in the early 1800’s by French military engineers who were asked to design magazine silos. They discovered that the base of the silo

supported only a portion of the total weight of the material and the sides of the silo carried more load compared to anticipated. Therefore they concluded that an invisible arch has formed within the silo structure. Later in 1895, this behavior observed in silos was utilized by Janssen to derive an approach to estimate arching effects in corn silos. In 1936 and 1943, Terzaghi conducted the most famous experimental (trap door experiment) and theoretical research of arching phenomena.

Definition of soil arching, in general, may be explained as the redistribution of soil forces resulting in lower stresses by which the soil load is transferred to a region of the soil mass. If a portion of a granular mass supported by a rigid retaining wall yields, the adjacent particles move with respect to remaining granular soil. This movement is resisted by shearing stresses that reduce the pressure on the translating part of the support while raising the pressure on the adjoining rigid regions. Rational methods and a better understanding of soil arching lead to technically economical and effective design structures in geotechnical applications. Since arching is a very complex phenomenon, utilization of numerical and experimental techniques in conjunction provides valuable insight to the soil arching behavior.

2.5 Analytical Modeling Studies on Soil Arching

Terzaghi performed the most well-known analytical studies on the arching effect in soil in 1936 and 1943. Terzaghi did not draw an arch in his studies to explain the phenomena, instead, used the term qualitatively. According to Terzaghi (1943), redistribution of stresses within the soil mass was described using “*trapdoor*” test setup. A trapdoor is a sliding or hinged door, at the same alignment with the surface of a floor or ceiling. The trap-door problem consists of mechanisms occurring in a cohesionless soil layer when a trapdoor located below is lowered. This movement results in a reduction of stresses in the adjacent soil mass. As soon as the panel is lowered, soil over the panel will tend to flow down as depicted in Figure 2-5. Stress due to the weight of the soil column over the moving panel will partially be carried by the adjacent soil in case the shear strength of the backfill is adequate. As a result, stresses in the surrounding soil will increase while the ones over the panel will decrease. The effect of arching, due to this reason, enables the design of buried structures and retaining walls to withstand lower loadings compared to the case when arching is ignored.

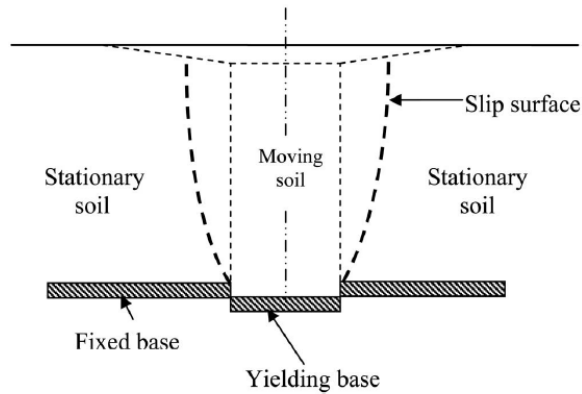


Figure 2-5 Stress redistribution in granular soil due to downward movement of a long narrow trapdoor resulting in soil arching (Terzaghi, 1943)

Deb (2010) investigated the arching behavior occurring on the stone columns installed in soft soils. Author stated that stress acting on soft soil decreases and stress on piles or columns increases due to soil arching depicted in Figure 2-5. In their study, a generalized analytical model was developed to examine the soil arching effect in stone columns applied to soft soil. The soft soil was idealized by using mechanical elements such as spring-dashpot system and the stone columns were represented by stiffer nonlinear springs. Plane strain condition was taken into account in the analysis. From the study it is observed that the degree of consolidation of soft soil, rigidity of the stone column, properties of soft soil and spacing between the stone columns considerably affect the degree of soil arching.

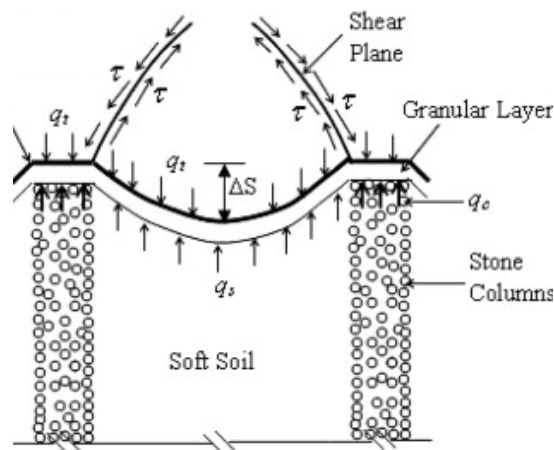


Figure 2-6 Soil arching mechanism in soft soil supported by stone column (Deb, 2010)

More detailed analytical approaches related to the soil arching behind earth retaining structures are given under Section 2.8.

2.6 Numerical Modeling Studies on Soil Arching

Chevalier et al. (2008) performed discrete element method (DEM) modeling to reproduce Terzaghi's well-known trap-door problem in order to understand the arching mechanism. DEM method has the ability to model the cohesionless materials as individual components

that can make and break contacts with its neighbors and able to analyze interacting bodies experiencing large relative movements. The method incorporates the friction between the elements and slipping takes place when the tangential force at contact goes over a critical value. In the case of a displacement, the equilibrium contact forces are determined from a series of calculations followed by force displacement law at each contact. When all forces in each contact are updated, forces and moment sums are determined on each element. This procedure is repeated in series. Therefore, especially for granular soil, DEM modeling gives results close to actual behavior. Authors modeled granular soil as composed of rigid particles that interact with each other through deformable contact points. Tangential and normal contact forces are encompassed by linear contact laws at each contact point.

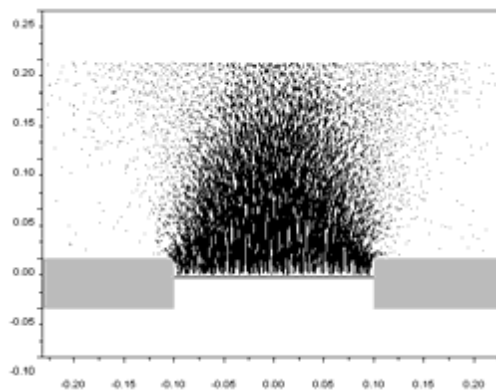


Figure 2-7 Displacement field of granular soil on the trap-door numerical modeling for $\delta=19$ mm (Chevalier et al., 2008)

Effects of frictional and size parameters were inspected and influence of particle shapes and grading were inspected in their study. Graphical representation of the displacement field within the granular soil placed on the trap-door calculated by discrete element method for $\delta=19$ mm is depicted in Figure 2-8. This study provided an important insight to the modeling of the soil arching effect in granular materials.

In a recent study, Nadukuru and Michalowski (2012) performed discrete element method (DEM) simulations of a prismatic sand heap using the PFC^{3D} code demonstrated in Figure 2-8 (a). This simulation was carried out using approximately 12,000 particles, of which 75% were spherical and 25% were clumps with an elongated shape. Soil arching effect can easily be observed in Figure 2-8 (b).

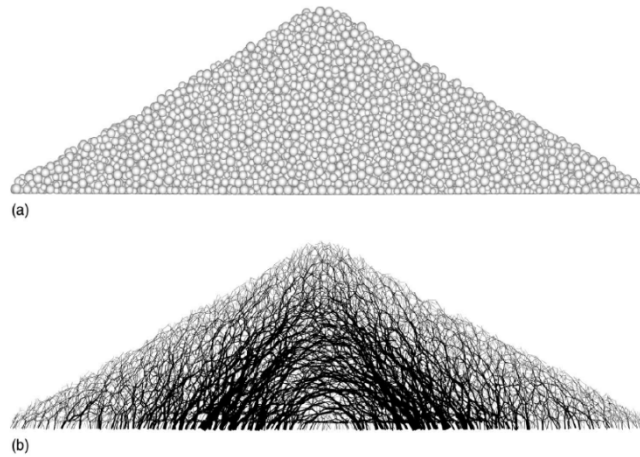


Figure 2-8 Discrete element modeling of (a) prismatic sand heap, (b) force chains
(Nadukuru and Michalowski, 2012)

In the numerical model given in Figure 2-9, rotation about the top edge was simulated. A rough wall with a coefficient of friction of $\mu=0.35$ was considered in the analyses. After the generation of the numerical model, rigid movement of the wall was induced. The displacements associated with the wall rotation about the top edge are illustrated in Figure 2-9.

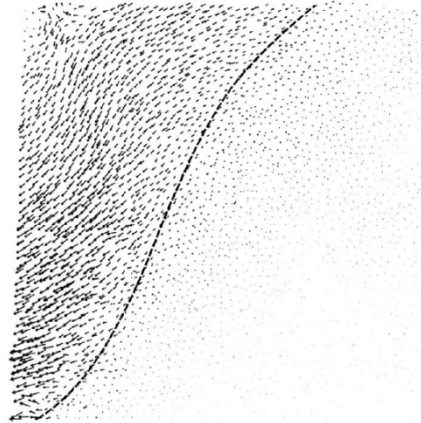


Figure 2-9 Displacements due to wall rotation of 0.008 radian about the top edge
(Nadukuru and Michalowski, 2012)

The force interactions between granular elements estimated from discrete element model are illustrated in Figure 2-9. It was observed that an arching effect similar to that seen in Figure 2-8 (b) occurs. This arching phenomenon is explained schematically in Figure 2-10. All displacement vectors tend to be parallel (not indicated on the figure) and inclined at an angle to a straight line that can be interpreted as a slip line behind a wedge for the case of translation and rotation about the base.

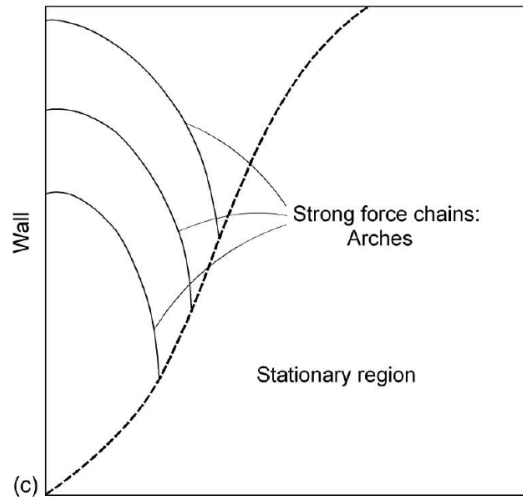


Figure 2-10 Arching phenomena interpreted schematically for the wall rotation about top (Nadukuru and Michalowski, 2012)

2.7 Physical Modeling Studies on Soil Arching

An experimental testing procedure was carried out by Costa et al., (2009) to analyze failure mechanisms induced within a deep rectangular trapdoor underlying granular material by the active soil movement. A schematic representation of the typical failure mechanism for different relative displacements (δ/B) is depicted in Figure 2-11. Failure mechanisms of the models were represented by a well-defined, single failure surface that is formed within the trapdoor. It is inferred from their investigation that the quantity of the self weight of the soil transferred to the base is a function of the shear characteristics of the base-soil interface and the geometry. Noteworthy dilation of the earth material located just above the trapdoor was observed during the failure mechanism.

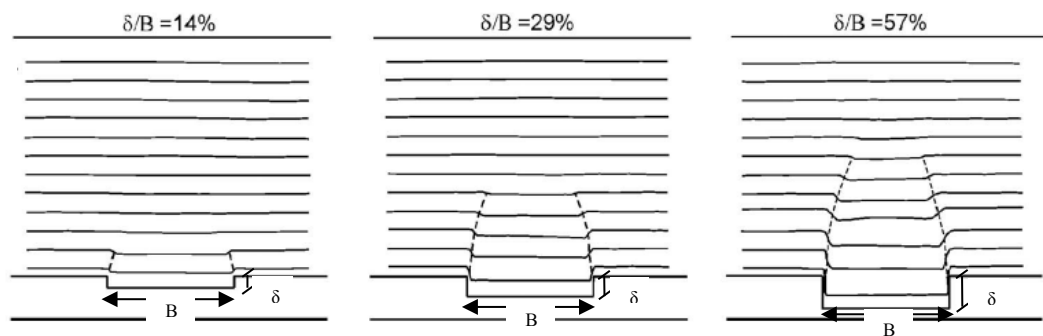


Figure 2-11 Observed failure mechanism in the granular soil for different relative displacements (δ/B) (Costa et al., 2009)

2.8 Analytical Studies on the Soil Arching Behavior

In 1895, Janssen built up a theoretical basis to understand arching phenomena by setting up a differential equation for lateral pressures in a grain silo filled with corn. In his approach, the force equilibrium for differential element within the bin was taken into

account and the ratio of vertical to horizontal stresses were taken as constant to simplify the problem. In a subsequent study, Marston (1930) suggested the first analytical formula for the average vertical normal stress within a cohesionless backfill in a long and narrow trench at any depth z as:

$$\sigma_v = \frac{\gamma B}{2\mu K} \left[1 - \exp\left(-\frac{2\mu K}{B} z\right) \right] \quad (2-2)$$

where μ = friction coefficient at the interface between wall and backfill which is equal to $\tan \delta$, (δ = friction angle at the wall-backfill interface), K = ratio of horizontal stress to vertical stress at the considered depth and B = width of the trench.

Author developed the expression by taking into account the equilibrium of an infinitesimal horizontal soil element and integrating over the height for plane strain case. K value proposed by Marston (1930) is equal to the ratio of the horizontal stress to vertical stress, and it is identical with the Rankine's active earth pressure coefficient:

$$K_a = \tan^2(45 - \varphi/2) = \frac{(1 - \sin \varphi)}{(1 + \sin \varphi)} \quad (2-3)$$

Subsequently, Terzaghi (1943) inserted the soil cohesion into the aforementioned expression and assumed that friction angle at the wall-backfill interface is equal to internal friction angle of the backfill, that is $\mu = \tan \varphi$ can be considered in the equation as:

$$\sigma_h = \frac{(\gamma B - 2c)}{2\mu} \left[1 - \exp\left(-\frac{2\mu K}{B} z\right) \right] \quad (2-4)$$

Terzaghi (1943) suggested that earth pressure coefficient (K) is constant at any point of the soil and it is an empirical value that can be up to 1.5. In his study, the graphical results demonstrating the arching effects were suggested for $K=1$ case. In a more recent study, Handy (1985) proposed an analytical expression by considering the reorientation for the principal stresses by the formation of a catenary arch due to soil arching in a trench. Handy assumed that cohesionless backfill is retained by two parallel, unyielding, rough vertical walls which is shown in Figure 2-12 (b). The arching effect partially supports the weight of the soil by inducing friction on the wall surface. In Figure 2-12 (a) minor principal stress planes drawn through the Mohr circle poles adapted from Krynine's solution (1945) indicate rotation of the major principal stress directions while the trajectory of minor principal stresses shows a continuous compression load within soil arches. Handy proposed Equation (2-5) for lateral earth pressures on the trench having a width of B :

$$\sigma_h = \frac{\gamma B}{2\mu} \left\{ 1 - \exp\left(-\frac{2K_w \mu}{B} z\right) \right\} \quad (2-5)$$

where $\mu = \tan \delta$ and K_w is given in Eq. (2-6) with $\theta_w = 45^\circ + \phi/2$ for rough vertical walls that is equal to Krynine's expression given in Eq. 2-7 and $\theta_w = 90^\circ$ for smooth walls that is equal to Rankine's lateral earth pressure coefficient (K) given in Eq. (2-3).

$$K_w = \frac{(\cos^2 \theta_w + K_a \sin^2 \theta_w)}{(\sin^2 \theta_w + K_a \cos^2 \theta_w)} \quad (2-6)$$

As indicated in Figure 2-13, partial arches within the slip plane rising at $45^\circ + \phi/2$ were taken into account to obtain the nonlinear pressure distribution behind retaining walls. Vertical stresses expressed in Eq. (2-2) were differentiated with respect to z to obtain Eq. (2-7) for horizontal earth pressure at any level behind a rigid rough wall:

$$\sigma_h = \frac{\gamma}{\mu} (H - z) \tan \left(45 - \frac{\phi}{2} \right) \left[1 - \exp \left(- \frac{K_w \mu}{\tan \left(45 - \frac{\phi}{2} \right)} \frac{z}{H - z} \right) \right] \quad (2-7)$$

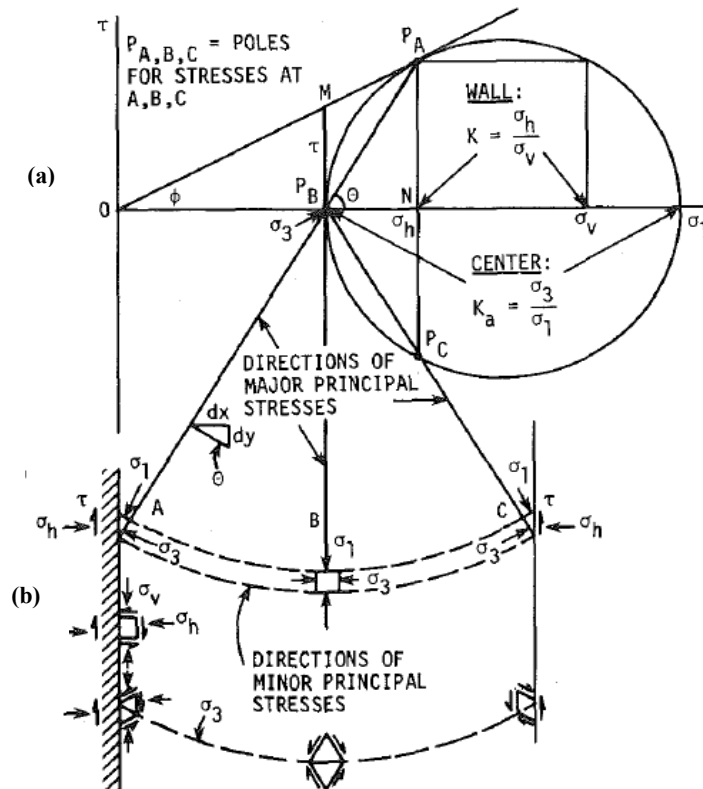


Figure 2-12 (a) Mohr circle representation of stresses due to soil arching close to the rough wall, (b) continuous inverted arch described as trajectory of minor principal stresses inside the vertical walled trench according to Krynine Approach (Handy, 1985)

Handy (1985) reported that the mobilization of friction on the wall-backfill interface results in an increase in the horizontal stresses and a decrease in vertical stresses. The rotation of principal stress directions results an increase in lateral earth pressure coefficients (K). Handy suggests that the actual value may be approximated by the lateral soil pressure coefficient at rest, K_0 given by Jaky (1944) as $K_0 = 1 - \sin \phi$. According to Krynine (1945), the lateral earth pressure coefficient $K_{Krynine}$ considering arching effects were calculated as follows by constructing the Mohr circles depicted in Figure 2-12.

$$K_{Krynine} = \frac{1}{1 + 2 \tan^2 \phi} = \frac{1 - \sin^2 \phi}{1 + \sin^2 \phi} \quad (2-8)$$

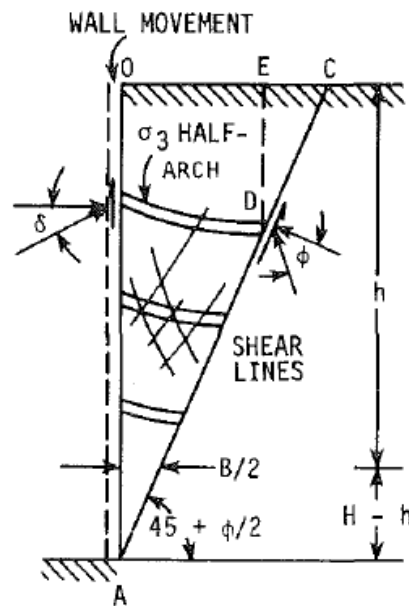


Figure 2-13 The graphical representation of lateral soil arching indicating the formation of catenary minor arches and shear lines for active stress conditions against a retaining wall (Handy, 1985)

In the same study, Handy (1985) explained that calculated vertical stress in the wall or conduit problems should be taken as the average vertical stress along the trench width. Therefore, K ratio is calculated as the horizontal stress over average vertical stress. Since the vertical stress close to the wall is lower than the average vertical stresses, it yields smaller K values if used in the calculations. The expression of K_w is as given in Equation (2-9),

$$K_w = (1.06)[\cos^2 \theta + (K_a) \sin^2 \theta] \quad (2-9)$$

In a more recent study, Wang (2000) proposed differential equations that lead to curvilinear lateral soil pressure distribution behind the retaining walls. In his study, effect of surcharge was taken into account. The equations were set up by considering a sliding soil wedge between a plane passing through the bottom edge of the retaining structure and the back of the wall having an angle of θ relative to the horizontal. Figure 2-14 shows the forces acting on an infinitesimal element taken from the wedge having a thickness of dy .

The solution of the equation gives a theoretical result for the unit soil pressure behind the retaining wall.

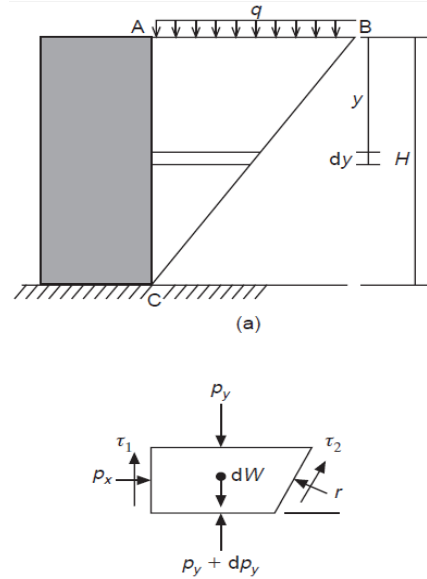


Figure 2-14 Forces acting on an infinitesimal element taken from the wedge (Wang, 2000)

The following assumptions were made in the solution of the differential equations:

$$\begin{aligned} p_x &= K p_y \\ \tau_1 &= p_x \tan \delta \\ \tau_2 &= r \tan \varphi \end{aligned} \quad (2-10)$$

where K is the lateral pressure coefficient, δ is the friction angle between the soil and the retaining wall and φ is the internal friction angle of the backfill.

Considering the equilibrium condition of both horizontal and vertical forces on the unit element, Wang obtained equation (2-11):

$$p_x = \frac{K_q q + K_y \gamma y}{\cos \delta} \quad (2-11)$$

where K_q is the surcharge coefficient and K_y is the backfill coefficient given in Eq. (2-12) and a is explained as;

$$\begin{aligned} a &= \frac{\cos(\theta - \varphi - \delta) \tan \theta}{\sin(\theta - \varphi) \cos \delta} \\ K_q &= K \left(\frac{H - y}{H} \right)^{aK-1} \end{aligned} \quad (2-12)$$

$$K_y = \left(\frac{K}{aK - 2} \frac{H - y}{y} \right) \left[1 - \left(\frac{H - y}{H} \right)^{aK-2} \right]$$

Wang (2000) reported that the lateral earth pressure has a curvilinear distribution and linear earth pressure distribution is a special case of his solution for $K=1/a$.

According to Paik and Salgado (2003), the equations suggested by Wang (2000) for the calculation of lateral active soil pressure has some shortcomings. They indicated that lateral earth pressure coefficients were not considered in Wang's solutions although it has a significant effect on the distribution lateral earth pressure. Additionally, lateral earth pressure expression given in Equation (2-8) gives K_w value of 1.06 for backfill internal friction angle of $\varphi=0^\circ$. However, this value should be equal to 1.0. This error reduces as φ and δ increase. The equations that were suggested by Paik and Salgado (2003) were derived from a physical problem where two rigid, parallel and rough vertical walls retain cohesionless material (Figure 2-15). One main assumption is that the settlement of the retained soil is adequate to induce full amount of friction between the wall-backfill interface. In Figure 2-15, the minor principal stresses (σ_3) on the differential flat element behind the retaining wall act throughout the concave arch, while the major principal stresses (σ_1) are perpendicular to the concave arch.

Paik and Salgado (2003) stated that the horizontal and vertical stress equations suggested by Handy (1985) possess some limitations. Although Handy (1985) explained that the horizontal and vertical stresses close to the wall at a depth z are related to the soil internal friction angle, φ and the interface friction angle between soil and wall, δ , these parameters were not considered in his derivations as can be seen in Equation (2-5). Paik and Salgado (2003) extended Handy's studies by including the effect of δ and φ on the vertical and horizontal stresses at depth z behind the retaining wall. To simplify the problem, a circular arch was considered unlike from Handy's solution given for a catenary arch shown in Figure 2-15. For the calculation of the active earth pressure on the wall, authors assumed that the failure surface for a rigid translating retaining wall is plane and have an inclination of $45^\circ+\varphi/2$ to the horizontal by taking full consideration of arching effects. Nevertheless, the slip surface behind the retaining wall is planar for $\delta=0$, but, for a rough retaining wall, that is $\delta\neq 0$, the failure line should be curved independent of the yielding mode (Terzaghi, 1943, Spangler and Handy, 1984).

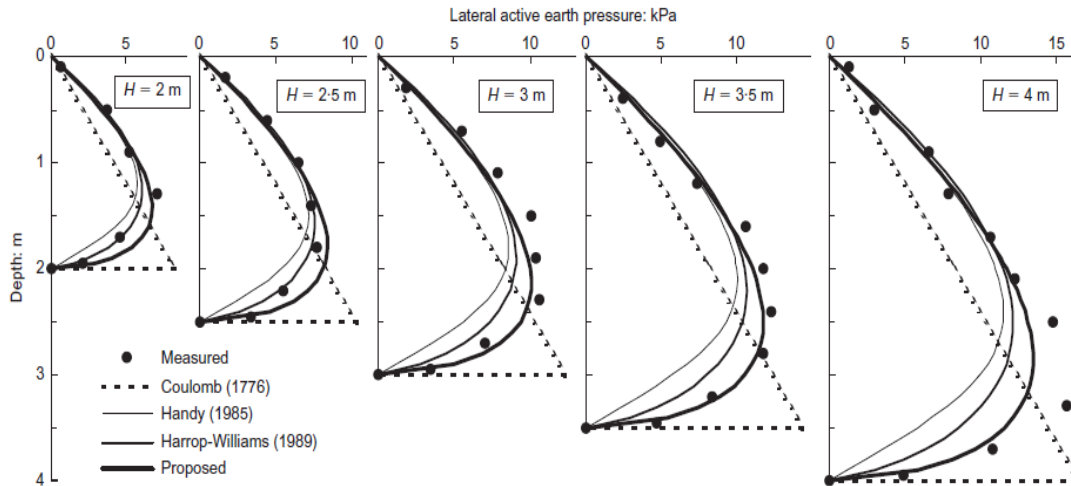


Figure 2-16 Comparison of measured and predicted active earth pressure distributions (Paik and Salgado, 2003)

2.9 Surcharge Induced Pressures Behind Retaining Walls

Surcharge type loads in the vicinity of the soil backfill causes additional lateral earth pressures on the retaining wall. Surcharge induced loads may occur from sloping backfill soils, footings of structure and adjacent vehicle loads supported by the backfill soil. The effect of surcharge on the retaining structure depends on the magnitude and location of the load relative to the wall. Proximity of the surcharge load to the retaining structure plays an important role on the surcharge induced lateral loads on the retaining walls. In general, if the distance from the retaining wall to surcharge load is more than the height of the wall, the effect of the surcharge will significantly diminish and practically it will have no effect on the lateral load acting on the retaining wall.

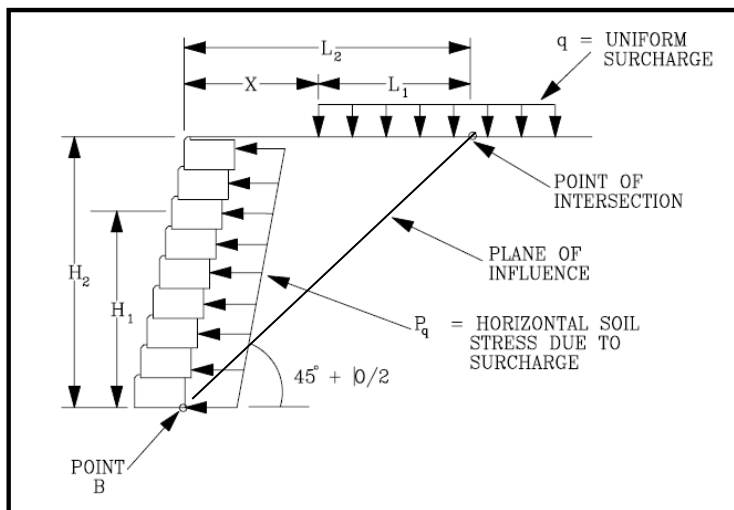


Figure 2-17 Effect of surcharge on retaining walls (AASHTO,1987)

In Figure 2-17 and Table 2-1, the effect of the surcharge on the retaining walls were explained (AASHTO, 1987). Surcharge load located along the upper surface of a

theoretical soil failure wedge possess considerable effect on the retaining wall. If surcharge load is located well beyond the failure wedge, it will have a negligible effect on the wall. Theories of earth pressure such as Rankine and Coulomb generally assume that stress due to surcharge is linearly increasing with depth and failure wedge has an angle of $45^\circ + \phi/2$. In addition to these assumptions, wall friction is neglected in the Rankine's lateral earth pressure theory.

Table 2-1 Effect of surcharge location on the retaining structure (AASHTO, 1987)

CASE 1 $X = 0$	CASE 2 $0 < X < L_2$	CASE 3 $X \geq L_2$
$P_q = (q) (K_a)$ Sliding Force: $F_s = (P_q) (H_2) \cos (\phi_w)$ Overturning Moment: $M_q = (0.5) (H_2) (F_s)$	$P_q = (q) (K_a)$ Sliding Force: $F_s = (P_q) (H_1) \cos (\phi_w)$ Overturning Moment: $M_q = (0.5) (H_1) (F_s)$	$P_q = 0$ Sliding Force: $F_s = 0$ Overturning Moment: $M_q = 0$

CHAPTER 3

ANALYTICAL MODELING OF SOIL ARCHING

3.1 Introduction

Estimation of the active lateral earth pressures is very important in the design phase of the retaining walls, especially for earth retaining walls. Civil engineers have traditionally calculated the active earth pressure against rigid retaining walls using either Coulomb's or Rankine's theories. Generally it is assumed that the distribution of active earth pressure acting upon the retaining wall is linear; however, many experimental results (Tsagareli, 1965 and Fang & Ishibashi, 1986) indicate that the distribution of active earth pressure behind a rough rigid wall is nonlinear. The nonlinearity of the active earth pressure distribution results from arching effects that was expressed by Handy in 1985.

Within the scope of this thesis study, a new analytical methodology is proposed to calculate lateral active earth pressures acting upon rigid retaining walls translating away from the backfill. In the proposed method, effect of surcharge was taken into account. In the proposed methodology, different combinations of soil failure wedge and lateral arch geometries are considered. In this context, a planar failure surface with parabolic concave soil arch is considered for the derivation of the horizontal stress distributions. This procedure is mentioned as *Method I*.

In the second approach, a curvilinear failure surface and circular soil arch segment is considered behind the rigid translating wall. The lateral pressure distribution relationships are formulated according to these assumptions and this approach is referred as *Method II*. As the last contribution, lateral active earth pressure expression which was formerly suggested by Paik and Salgado (2003) is extended to include surcharge effects on the lateral earth pressures.

For the derivation of *Method I*, parabolic concave arch and linear failure wedge is considered for the derivations. However, many experimental results (Tsagareli, 1965, Fang & Ishibashi (1986) pointed out that the shape of the slip surface is curved irrespective of the yielding mode according to Terzaghi (1943). Considering the data obtained from physical modeling studies, *Method II* is proposed by adopting a parabolic failure surface to the Paik and Salgado (2003) approach.

3.2 Lateral Earth Pressure Distribution Considering Planar Failure Surface and Circular Soil Arch Formation within the Failure Zone

To determine the active earth pressure acting on a rigid retaining wall, Paik and Salgado (2003) derived an expression given in equation (2-13) considering the simplifying assumption that the slip surface assumed to be linear. In their study, a rough rigid retaining wall that translates horizontally away from the soil is considered as given in Figure 3-1.

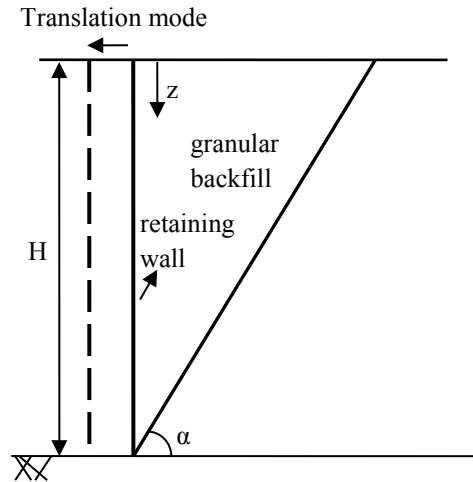


Figure 3-1 Rigid retaining wall that translates horizontally away from the soil

Lateral active earth pressure expression proposed by Paik and Salgado (2003) is obtained by the summation of all vertical forces on the differential element given in Figure 2-15 as:

$$\left[\bar{\sigma}_v + \frac{\gamma}{1 - K_{aw} \tan \delta \tan \alpha} (H - z) \right] (H - z)^{-K_{aw} \tan \delta \tan \alpha} = C \quad (3-1)$$

where K_{aw} was defined as coefficient of lateral active pressure on wall expressed in equation (2-13), α is defined same with Coulomb's theory as $45^\circ + \phi/2$ and C is an integration constant. In order to examine the influence of the surcharge, a modification to Paik and Salgado's theory is done in this work to include the effect of surcharge into Equation (3-1). This procedure is described in the next section.

3.3 Modification of Paik and Salgado Lateral Soil Arching (2003) Approach Assuming Planar Failure Surface and Parabolic Soil Arch within the Backfill (Method I)

In this section, a differential flat soil element within the extent of the failure wedge is taken into account to obey equilibrium equations. With horizontal translation of the wall, the flat element takes the form of an arc of a parabolic arch in order to calculate lateral active earth pressures based on Handy's approach. The parabolic arch occurs when a uniform load (the weight of soil) is applied on the arch, causing the internal compression

of the soil element due to vertical forces. In order to determine the active lateral stress acting on the rigid translating retaining wall, the assumptions made by Paik and Salgado (2003) is taken into account. Accordingly, two parallel rigid vertical walls retaining granular backfill is considered as illustrated in Figure 2-14. It is assumed that settlement of the retained soil is large enough to fully induce friction between the walls and soil. Due to the frictional forces, the weight of the differential flat element within the soil mass is partially supported. This frictional forces result in changes in the direction of the principal stresses acting on differential flat element. Major principal stresses, σ_1 , on the differential flat element depicted in Figure 3-2 are applied normal to the concave arch and become horizontal at the center of the element according to Handy (1985). Similarly, if a rigid rough retaining wall moves away from the soil horizontally, the direction of the major and minor principal stresses on the differential flat element change due to frictional force at the wall-backfill interface.

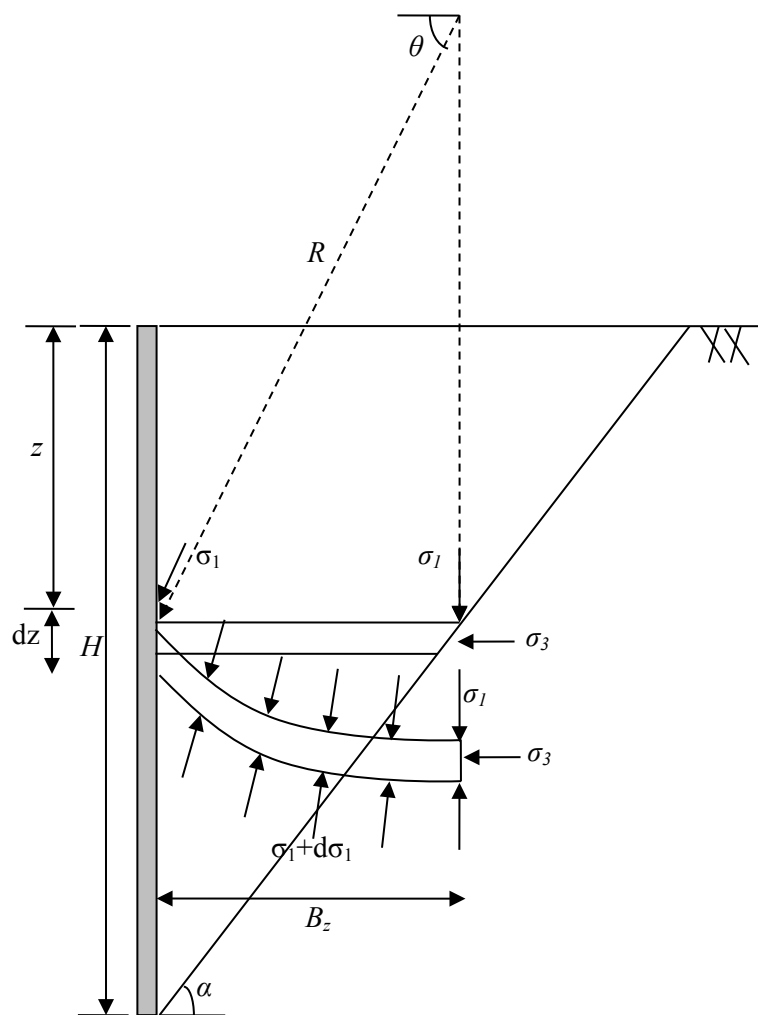


Figure 3-2 Directions of the major and minor principal stresses on the differential parabolic element in the granular backfill behind rigid retaining wall

The major principal stresses, σ_1 , are applied perpendicular to the concave arch whereas the minor principal stresses, σ_3 , on the differential flat element behind the wall act along the

concave arch as shown in the Figure 3-2. This figure illustrates the movement of the lateral flat soil element when the retaining wall translates. For the derivation of Method I, The assumption of Coulomb's theory that the slip surface is to be plane at an angle of $45^\circ + \phi/2$ to the horizontal is used considering arching effects in backfill. The shape of the concave arch is considered to be parabolic as indicated in the figure. In this case, the width B_z of the differential flat element can be defined as:

$$B_z = R \cos \theta \tag{3-2}$$

where R is the radius of the minor principal stress trajectory defined in Eq. (3-13) and θ is the rotation angle of the principal stresses for the wall.

When the horizontal force equilibrium on the differential flat element illustrated is considered, the active lateral stress σ_{ahw} on the wall can be expressed by using trigonometric relations at point 'A' in Figure 3-4 expressed in Eq. (3-3) as:

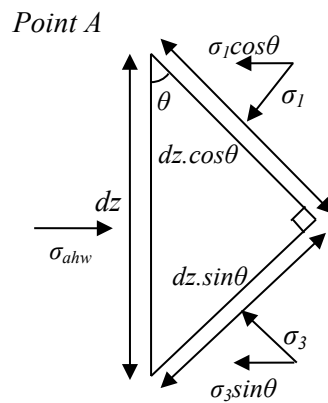


Figure 3-3 Trigonometric relations at point A to obtain active lateral stress ratio, σ_{ahw} , on wall

$$\sigma_{ahw} dz = \sigma_1 \cos^2 \theta dz + \sigma_3 \sin^2 \theta dz \tag{3-3}$$

which is equal to, $\sigma_{ahw} = \sigma_1 \cos^2 \theta + \sigma_3 \sin^2 \theta$ (3-4)

$$\frac{\sigma_v}{\sigma_1} = \sin^2 \psi + \frac{1}{N} \cos^2 \psi \quad (3-8)$$

The lateral and vertical soil pressures acting at an arbitrary point along a differential flat element within the backfill is calculated using Equation (3-6) and Equation (3-8).

3.3.1 Determination of the Rotation angle, θ

Rotation angle of major and minor principal stresses for retaining wall with a friction angle of $\delta \leq \phi$ can be obtained by means of Mohr circle representation as depicted in Figure 3-5. From trigonometry of PBC and OPB, shown in the figure, the following equation is obtained:

$$\tau_w = \sigma_{ahw} \tan \delta = (\sigma_{ahw} - \sigma_3) \tan \theta \quad (3-9)$$

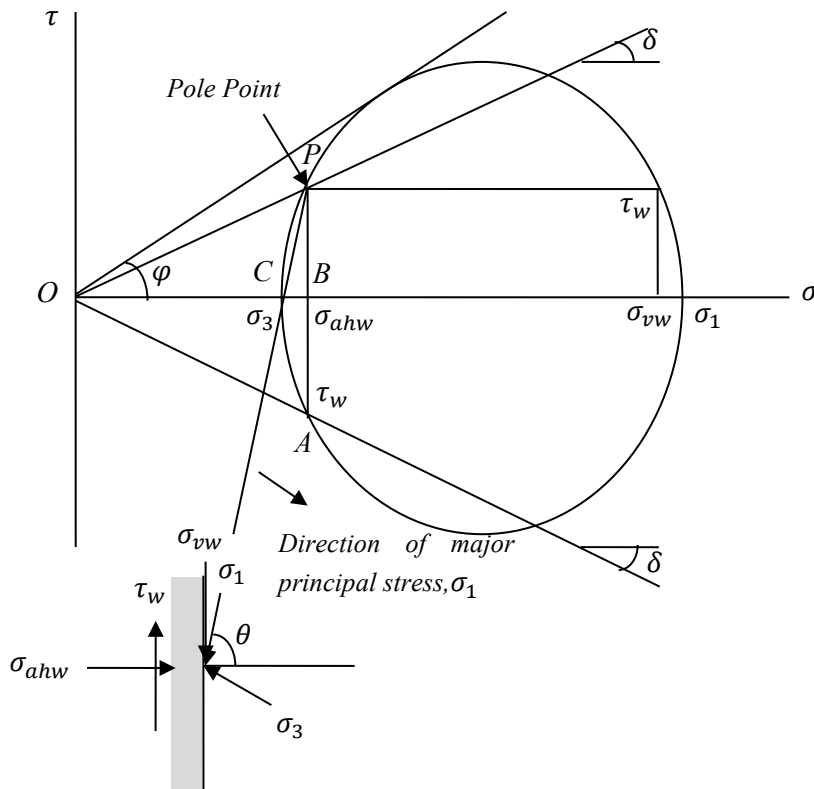


Figure 3-5 Mohr circle to determine the rotation angle, θ

From Eq.(3-9), $\tan \theta$ is obtained as:

$$\tan \theta = \frac{(\sigma_{ahw}/\sigma_3)}{(\sigma_{ahw}/\sigma_1) - 1} \tan \delta \quad (3-10)$$

Dividing equation (3-10) by σ_3 yields:

$$\frac{\sigma_{ahw}}{\sigma_3} = N \cos^2 \theta + \sin^2 \theta \quad (3-11)$$

Substitution of equation (3-11) into equation (3-10) results in the following second-order relationship:

$$\tan \theta = \frac{N + \tan^2 \theta}{N - 1} \tan \delta \quad (3-12)$$

where $N = \tan^2(45^\circ + \varphi/2)$. θ is given in Eq.3-13, (see Appendix for detailed derivation)

$$\theta = \tan^{-1} \left[\frac{(N - 1) \pm \sqrt{(N - 1)^2 - 4N \tan^2 \delta}}{2 \tan \delta} \right] \quad (3-13)$$

where δ is the wall friction angle. The larger of the two values accounts for the active condition of the retaining wall.

The main difference between the current method and Paik-Salgado Approach is the assumption of parabolic concave soil arch within the failure wedge. A new relationship for lateral earth pressure coefficient (K) value considering lateral arching is set up by dividing the active lateral stress on the wall to the average vertical stress. Within the derivation of the equations proposed in the current study, a parabolic arch is expressed in polar form. Any point on the parabolic arch is represented as (r, ψ) and the left boundary point of the parabolic arch which is on the wall is represented by (R, θ) . The general equation for the parabolic arch is defined as:

$$R = \frac{2\beta}{1 - \cos \psi} \quad (3-14)$$

where β is the parameter defining the shape of parabolic arch. The differential vertical force, dV , depicted in Figure 3-4 is obtained as:

$$dV = \sigma_v \cdot dA = \sigma_1 \left(\sin^2 \psi + \frac{\cos^2 \psi}{N} \right) (R \sin \psi d\psi) \quad (3-15)$$

where dA is the width of the shaded element at point B illustrated in Figure 3-4.

3.3.2 Determination of lateral soil pressure acting on retaining wall

The average vertical stress $\bar{\sigma}_v$ is obtained by dividing the total vertical force, V , acting on the differential flat element by the width of the differential flat element, $B_z = R \cos \theta$ where R is defined in equation (3-14). In this case, average vertical stress can be defined as:

$$\bar{\sigma}_v = \frac{V}{B_z} = \int_{\theta}^{\pi/2} \frac{dV}{B_z} = \int_{\theta}^{\pi/2} \frac{[\sigma_1(\sin^2 \psi + \cos^2 \psi/N)(2\beta \sin \psi)d\psi]}{\left\{(1 - \cos \psi) \left[\frac{2\beta \cos \theta}{1 - \cos \theta} \right]\right\}} \quad (3-16)$$

Integrating the equation (3-16) with respect to the angle ψ from θ to $\pi/2$ yields the following relationship:

$$\bar{\sigma}_v = [\sigma_1(1 - \cos \theta)] \left\{ 1 + 0.5 \cos \theta - (1/N) \left[1 + 0.5 \cos \theta + \log \left(\frac{1 - \cos \theta}{\cos \theta} \right) \right] \right\} \quad (3-17)$$

Lateral earth pressure coefficient (K_{ap}) for planar failure surface with parabolic concave arch was obtained by the division of equation (3-5) by Eq. (3-17) to obtain Eq. (3-18);

$$K_{ap} = \frac{[\cos^2 \theta + (\frac{1}{N}) \sin^2 \theta]}{\left\{ (1 - \cos \theta) \left[1 + 0.5 \cos \theta - (1/N) \left(1 + 0.5 \cos \theta + \log \frac{(1 - \cos \theta)}{\cos \theta} \right) \right] \right\}} \quad (3-18)$$

The proposed relationship takes into account the variation of $\bar{\sigma}_v$ with φ and δ . All of the forces exerted on the differential flat element having a thickness of dz are illustrated in Figure 3-6. These are the shear stresses, τ_w , along the wall, self weight of the differential element and the average vertical stresses, $\bar{\sigma}_v$. Shear stress along the wall is expressed as:

$$\tau_w = \sigma_{ahw} \tan \delta \quad (3-19)$$

Summation of all vertical forces yields the following expression:

$$d\bar{\sigma}_v B_z + \bar{\sigma}_v K_{ap} \tan \delta dz = \gamma B_z dz \quad (3-20)$$

where γ is the total unit weight of the soil and K_{ap} is the new active lateral stress ratio that takes into account arching effects explained in Eq. (3-18). As shown in Figure 3-5, the major and minor principal stresses at the right edge of the differential element act in the vertical and horizontal directions, respectively. Hence, the shear stresses in the horizontal and vertical planes at the right edge of the differential flat element are equal to zero. On the other hand, there is nonzero shear stress along the wall due to the frictional forces induced at the left edge of the differential element due to wall-backfill interface friction. It should be noted that the shear stress in a vertical plane is zero at the right edge of the element.

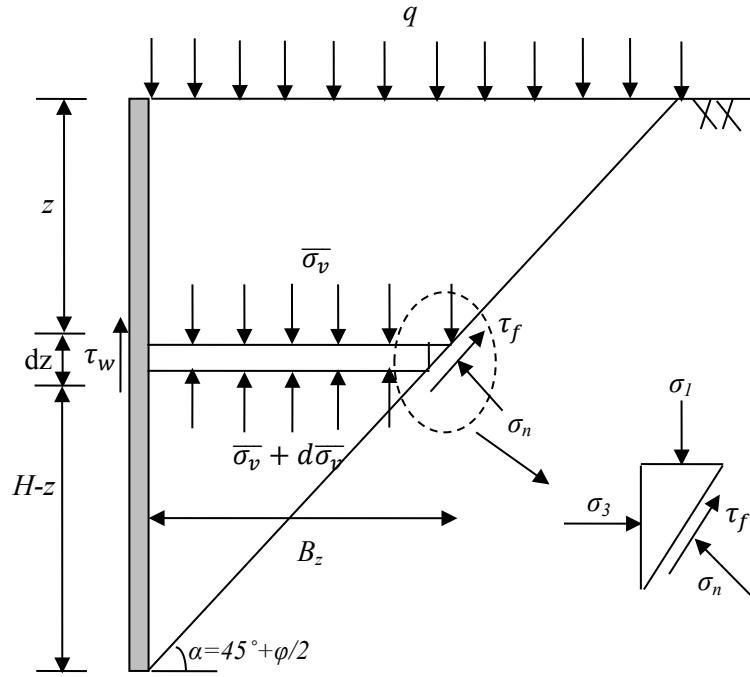


Figure 3-6 Free body diagram of differential flat element with planar failure surface for Method I

Substituting B_z into Equation (3-20) yields the following relationship:

$$d\bar{\sigma}_v + \bar{\sigma}_v K_{ap} \tan \delta \tan \alpha \frac{dz}{(H-z)} = \gamma dz \quad (3-21)$$

Integrating the differential equation given above results in the general solution:

$$\left[\bar{\sigma}_v + \frac{\gamma}{1 - K_{ap} \tan \delta \tan \alpha} (H-z) \right] (H-z)^{-K_{ap} \tan \delta \tan \alpha} = C \quad (3-22)$$

that is same with equation (3-1). It should be noted that the general lateral earth pressure acting on rigid translating retaining wall is independent of the shape of the arch. However, the lateral earth pressure coefficient (K_{ap}) in Eq. (3-18) is different from the one suggested by Paik and Salgado (2003). In the current study, K_{ap} value is calculated from parabolic arch and planar failure surface assumption which is different from K_{av} value proposed in Paik and Salgado's (2003) study.

The average vertical stress at any depth is obtained by applying the boundary condition $\bar{\sigma}_v = 0$ at $z = 0$ to Eq. (3-22). The expression to obtain lateral active horizontal stress acting on rough rigid translating retaining walls including surcharge is identical with Equation (3-29) however the active lateral stress ratio is different in this case as explained above.

3.4 Modification of Paik and Salgado Lateral Soil Arching (2003) Approach Assuming Curvilinear Failure Surface and Circular Soil Arch in Backfill (Method II)

As discussed in the literature review chapter, the assumption of linear slip surface behind the retaining wall is more suitable if the wall-backfill interface friction angle is taken as zero ($\delta=0$); however, there is always friction between the retaining structure and the retained backfill material in reality. The presence of vertical friction along the wall causes lateral soil arching within the soil wedge by mobilizing soil shear strength along soil arches. This behavior significantly affects the lateral earth pressures as presented in chapter 4.

For a rough rigid wall having $\delta \neq 0$, the critical failure surface is curved independent of the yielding mode (Terzaghi, 1943, Spangler & Handy, 1984). In this method, expressions are derived with the assumptions of curvilinear failure surface and circular soil arch along the failure mass. For the derivations, boundary conditions suggested by Spangler and Handy (1984) are adopted. The planar and parabolic failure surfaces are illustrated in Figure 3-7.

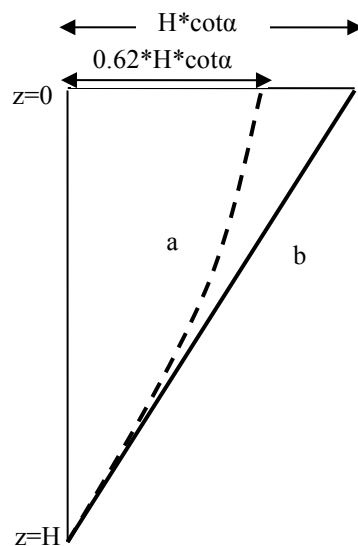


Figure 3-7 Schematic representation of two different failure surfaces (a) parabolic (b) planar failure surface

3.4.1 Parabolic failure surface with Spangler-Handy's boundary conditions

For the derivation of lateral earth pressure expressions indicated as *Method II*, a parabolic failure wedge (Figure 3-8) with an equation of:

$$z = ax^2 + bx + c \tag{3-23}$$

is considered. The parabola that makes an angle of $45^\circ + \phi/2$ degrees with horizontal and the bottom, and the boundary conditions are taken as follows;

$$\frac{dz}{dB} = \tan \alpha \text{ for } z=H, \quad B = 0 \text{ for } z = H, \quad B = A.H.\cot \alpha \quad (3-24)$$

where A is taken as constant and equal to 0.62 according to the experimental results suggested by Tsagareli (1965). This constant is defined in Eq. (3-25) and it expresses the ratio of the width of failure plane at backfill surface for parabolic failure wedge to the width of failure plane at the backfill surface for planar failure wedge.

$$A = \frac{B_{parabolic}}{B_{planar}} \quad (3-25)$$

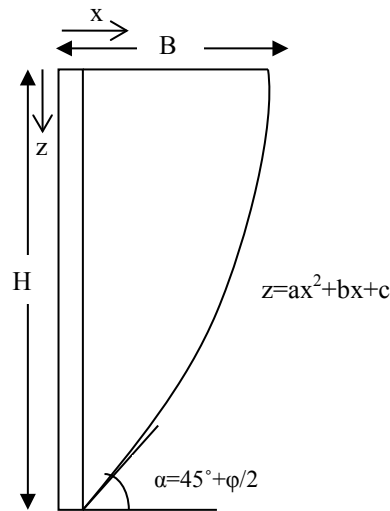


Figure 3-8 Parabolic failure surface with Spangler-Handy Boundary Conditions

The constants a , b and c which appear in Eq. (3-23) were solved as follows using the boundary conditions adopted from Spangler and Handy (1984):

$$a = \left(\frac{A-1}{A^2}\right) \left(\frac{\tan^2 \alpha}{H}\right); \quad b = -\tan \alpha; \quad c = H \quad (3-26)$$

Lateral earth pressures acting on retaining wall having height of H are calculated by taking horizontal slices within the curvilinear failure surface. A graphical illustration of the method is in Figure 3-9. The height of the wall is divided into ' n ' number of horizontal slices with a thickness of $\Delta z = z_i - z_{i-1}$. The failure surface makes angles of α_i and α_n with the vertical at top and bottom, respectively while i goes from 1 to n , $i = 1, 2, 3, \dots, n$.

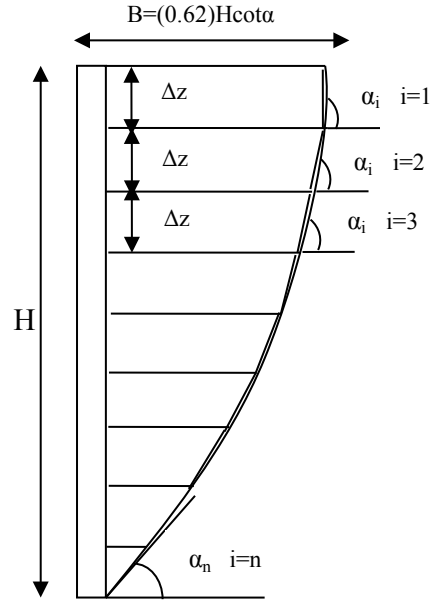


Figure 3-9 Graphical depiction of horizontal slices within parabolic failure surface with Spangler and Handy's (1984) boundary conditions

The rate of change of failure angle (α_i to α_n) is calculated according to the following formula given in Equation (3-26) as;

$$\alpha_i = \frac{\pi}{2} - \left\{ \tan^{-1} \left[\frac{\sqrt{b^2 - 4 \cdot a \cdot (c - z_i)} - \sqrt{b^2 - 4 \cdot a \cdot (c - z_{i-1})}}{2 \cdot a \cdot (z_i - z_{i-1})} \right] \right\}, i = 1, 2, \dots, n \quad (3-27)$$

where $z_i = (H \cdot i/n)$ and n is the number of horizontal slices (Visit Appendix for detailed derivation). Lateral active earth pressures including arching effect is obtained similarly with the procedure described in Section 3.2 previously. It was assumed that the trajectory of minor principal stresses takes the form of a circle. Nevertheless, since the height of the retaining wall was divided into number of n small slices, lateral active earth pressure was calculated according to the following formula;

$$f(\sigma_{ahw}) = \begin{cases} \sum_{i=1}^{n-1} \sigma_{ahw} = \frac{\gamma \cdot H \cdot K_{aw}}{1 - (K_{aw} \cdot \tan \delta \cdot \tan \alpha_i)} \left[\left(1 - \frac{z_i}{H}\right)^{K_{aw} \cdot \tan \delta \cdot \tan \alpha_i} - \left(1 - \frac{z_i}{H}\right) \right] & \text{for } i = 1, 2, \dots, n-1 \\ \sum_{i=n-1}^n \sigma_{ahw} = (0.97) \cdot \sigma_{ahw, z=0.9H} & \text{for } i = n \end{cases} \quad (3-28)$$

where K_{aw} was defined in Equation (2-12) for circular concave soil arch. However, the lateral pressure for the last slice is multiplied by a constant of '0.97' to obtain a better fit with the physical test results. This ratio was taken from the experimental test results performed by Fang and Ishibashi (1986) as the horizontal active stress value next to last

slice divided by the horizontal stress ratio obtained at the base of the retaining wall. Based on the data obtained from physical model tests performed by Fang and Ishibashi (1989), lateral pressure at the wall base can be considered as 97% of the lateral pressure at a depth of approximately 0.9H from wall top.

3.5 Modification of Paik and Salgado Lateral Soil Arching (2003) Approach to Include Surcharge Effect on the Lateral Earth Pressure Distribution

To obtain Equation (2-13), average vertical stress at any depth is obtained by applying the boundary condition $\bar{\sigma}_v = 0$ at $z = 0$ to Equation (3-1). In this topic, so as to examine the effect of surcharge, a new formula is developed by applying the boundary condition of $\bar{\sigma}_v = q$ at $z = 0$ to Equation (3-1). New expression to obtain lateral active horizontal stress acting on rough rigid translating retaining walls including surcharge is derived as follows:

$$\sigma_{ahw} = \left(\frac{\gamma H K_{aw}}{1 - K_{aw} \tan \delta \tan \theta} \right) \left[\left(1 - \frac{z}{H} \right)^{K_{aw} \tan \delta \tan \theta} - \left(1 - \frac{z}{H} \right) \right] + \left[q K_{aw} \left(1 - \frac{z}{H} \right)^{K_{aw} \tan \delta \tan \theta} \right] \quad (3-29)$$

The substeps leading to (3-29) are presented in the Appendix. Comparison of the lateral earth pressures calculated by this formula with those of the previous studies is discussed in detail in the next chapter. In this equation, trajectory of minor principal stresses is found to take the form of an arc of a circle. However, the shape of the concave arch is inferred to be in catenary shape, elliptic or parabolic according to Livingston (1961), Walker (1966) and Handy (1985).

CHAPTER 4

PARAMETRIC STUDY

4.1 Introduction

In this chapter, results of a parametric study were presented to discuss the influence of the following parameters:

- i. internal friction angle (φ) of the backfill soil
- ii. friction angle (δ) between the wall and backfill
- iii. wall height (H)

on lateral pressure distribution, total active thrust and the application point of the total active thrust. Results obtained from proposed methodologies are compared to those estimated with different theories of earth pressure. Influence of the shape of critical failure surface and the lateral soil arch induced within the backfill are investigated within the parametric analyses.

4.2 Parametric Analyses Regarding the Distribution of Lateral Active Soil Pressures

Lateral pressure distributions estimated by the proposed methodologies are validated against physical test data and compared with the predictions of previous earth pressure theories. Proposed analytical model are further calibrated for a better fit with the actual test data at the vicinity of the wall base. Effect of internal friction angle, wall-backfill interface friction angle and retaining wall height are investigated within the parametric study.

4.2.1 Lateral Active Soil Pressures

To validate the predictions obtained from Method I and Method II, results are compared with field test results of Tsagareli (1965) and physical test data presented by Fang & Ishibashi (1986). Figure 4-1 shows the distributions obtained using the analyses of Coulomb (1776), Rankine (1857), Handy (1985), Wang (2000) and Paik & Salgado (2003). Pressure distributions predicted by Method I and Paik-Salgado Approach (2003) are obtained by using lateral active earth pressure coefficients given in Equations (2-13) and (3-18) respectively, whereas those of Handy (1985) and Wang (2000) theories are calculated by means of Equations (2-7) and (2-11), respectively.

Tsagareli (1965) suggests zero horizontal active earth pressure at the base of the retaining wall as illustrated in Figure 4-1. Physical test results carried out by Tsagareli (1965) and Fang & Ishibashi (1986) exhibit different modes of lateral earth pressure distributions. On the other hand, Rankine’s theory does not take into account the effects of soil – wall interface friction angle. Hence, in Figure 4-2, test data of Tsagareli and earth pressures estimated by Rankine’s theory are removed from Figure 4-1 to provide simplicity.

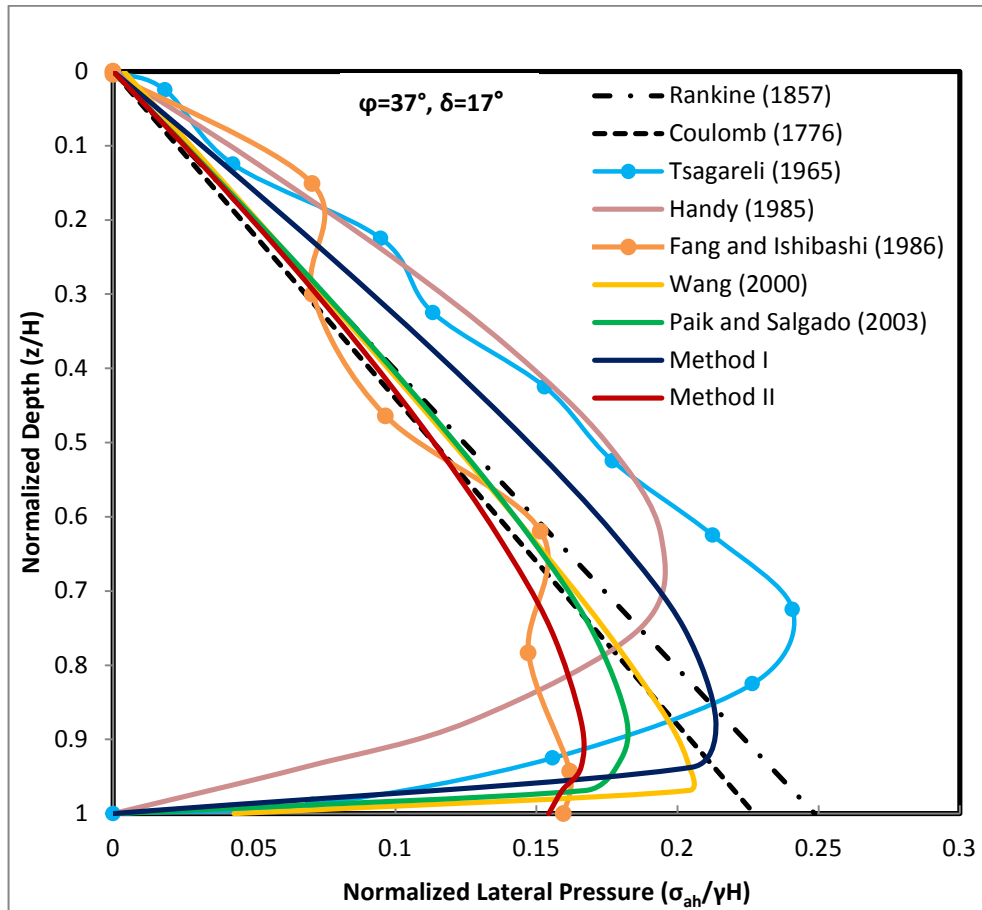


Figure 4-1 Comparison of lateral active earth pressure distributions predicted with different methods and physical test results

The unit weight of the backfill material used in physical tests was reported as 15.4 kN/m³ whereas φ and δ were indicated as 37° and as 17°, respectively (Fang and Ishibashi, 1986). In Figure 4-2, similar values were taken into account while calculating the normalized lateral earth pressures. It is observed that the lateral earth pressure distributions estimated by the proposed methods and the physical tests are curvilinear whereas those predicted by Rankine’s or Coulomb’s theory are linear and pressures estimated by Rankine’s theory constitute an upper bound for Method I. Actual test data clearly indicates the nonlinear nature of the earth pressure distribution. According to Method I and Handy (1985), highest lateral earth pressures are observed at 90% and 70% of the normalized depth, respectively. Investigation of the Figure 4-2 indicates that Method II makes the best estimation of the actual test results.

Method I over predicts lateral stresses since K_{ap} which is defined as the active lateral earth pressure ratio for parabolic concave arch given in Equation (3-18), provides relatively high active lateral stress ratios. On the other hand, both Method I and Method II provide more satisfactory values compared to Coulomb's theory since the proposed methods take into the account the effect of arching through the lower part of the retaining wall.

In Figure 4-3, effect of vertical surcharge load in the wall vicinity is shown by presenting lateral soil pressure distributions along wall height. Surcharge load was taken as $q = \gamma H$. Lateral earth pressures indicated in Figure 4-3 are normalized with respect to unit weight of the backfill material times the height of the wall.

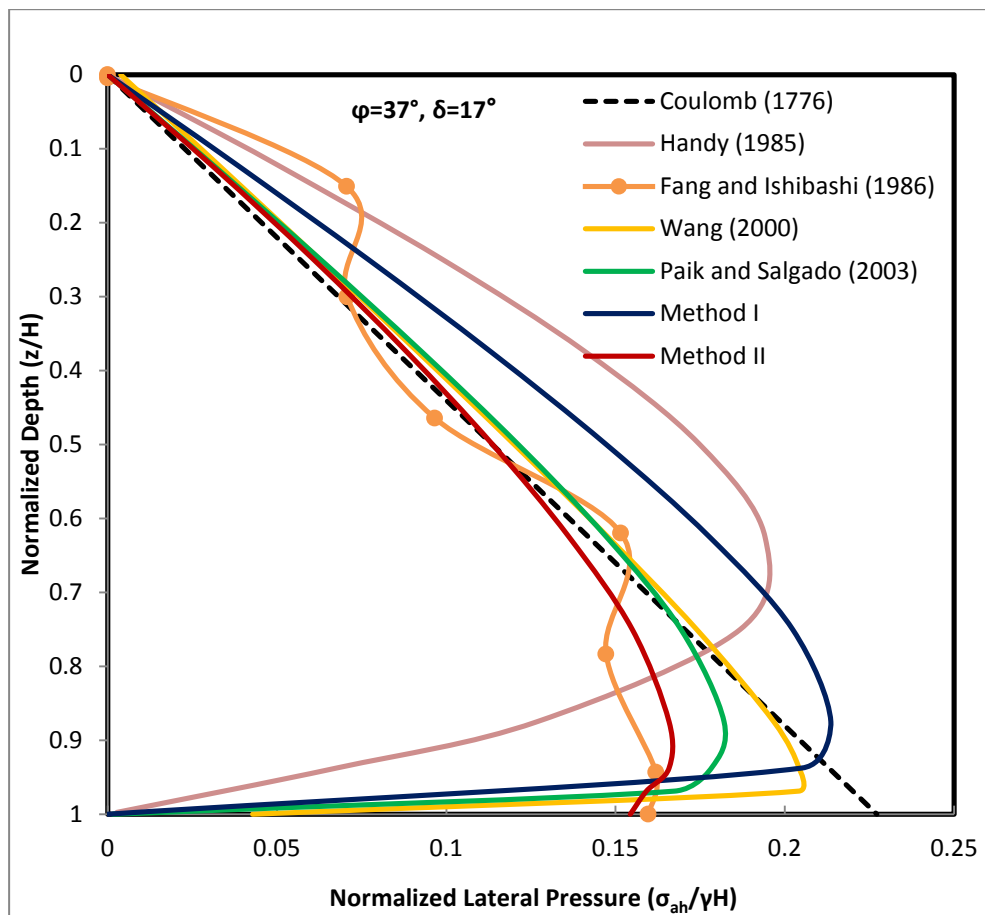


Figure 4-2 Comparison of lateral active earth pressure distributions predicted with different methods with the physical test results (Data of Tsagarelli, 1965 and Rankine's theory are removed from the previous figure).

It is observed that the distribution of lateral active earth pressures including surcharge are consistent with those depicted in Figure 4-2. Stresses calculated by Method I provide relatively large values since active lateral earth pressure ratios are significantly higher in this method. Lateral earth pressures calculated at $z=0$ is different for all of the approaches except Method II and Paik-Salgado Approach since the lateral earth pressure coefficients estimated by these methods are similar.

Predictions of Method II provide a lower bound for Wang and modified Paik-Salgado approaches whereas predictions of Method I give an upper bound. Although Method II and Modified Paik and Salgado approaches give the same lateral normalized stress ratios at the wall top, Method II estimates lower stress ratios along the wall height since it considers the shape of the critical failure line as parabolic whereas modified Paik and Salgado approach assumes a planar failure surface as shown in Figure 3-7. Although the critical failure lines make an angle of $\alpha = 45^\circ + \varphi/2$ with horizontal at the base of the retaining wall height for both approaches, Method II predicts lower horizontal stress values since a parabolic critical failure surface is assumed in this approach. Shape of the failure surface affects the amount of mobilized soil shear strength and also the weight of the active soil wedge.

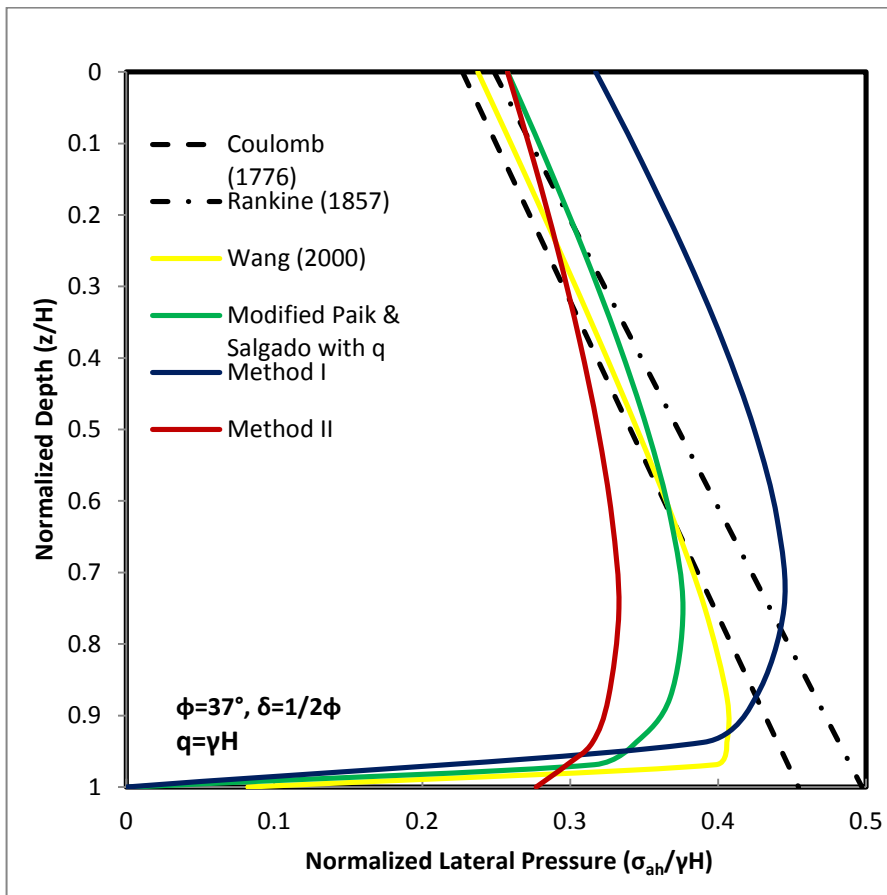


Figure 4-3 Comparison of surcharge induced lateral active earth pressures for different approaches

Additionally, the lateral earth pressure distribution proposed by Wang (2000) results in a different shape compared to the other approaches. This is due to the fact that Wang do not take into account a suitable lateral earth pressure coefficient although the lateral earth pressure coefficient has a significant effect on the distribution of the lateral earth pressures as explained by Paik and Salgado (2003). In his study, a closed form solution for the lateral earth pressure coefficient is not suggested. The analyses are carried out by making assumptions for K values.

4.2.2 Effect of internal friction angle on lateral active earth pressures

In Figure 4-4, the effect of internal friction angle on the lateral active earth pressure distribution behind a rigid translating retaining wall is illustrated for a wall-backfill friction angle of $\delta = 1/2\phi$ and internal friction angles between $\phi = 0^\circ$ and $\phi = 40^\circ$. In practice, results are mostly applicable to internal friction angles higher than 20° which are commonly encountered for granular soils. The pressure distribution becomes more non-linear as the internal friction angle of the soil increases from $\phi = 0^\circ$ to $\phi = 40^\circ$. It is also observed that the active earth pressure behind the retaining wall decreases as the internal friction angle of the soil increases. Method I gives higher lateral active earth pressures compared to Method II for the same internal friction angle. Besides, Method II gives non-zero pressure values at the base of the retaining wall which exhibits a better agreement with the physical test results carried out by Fang & Ishibashi (1986).

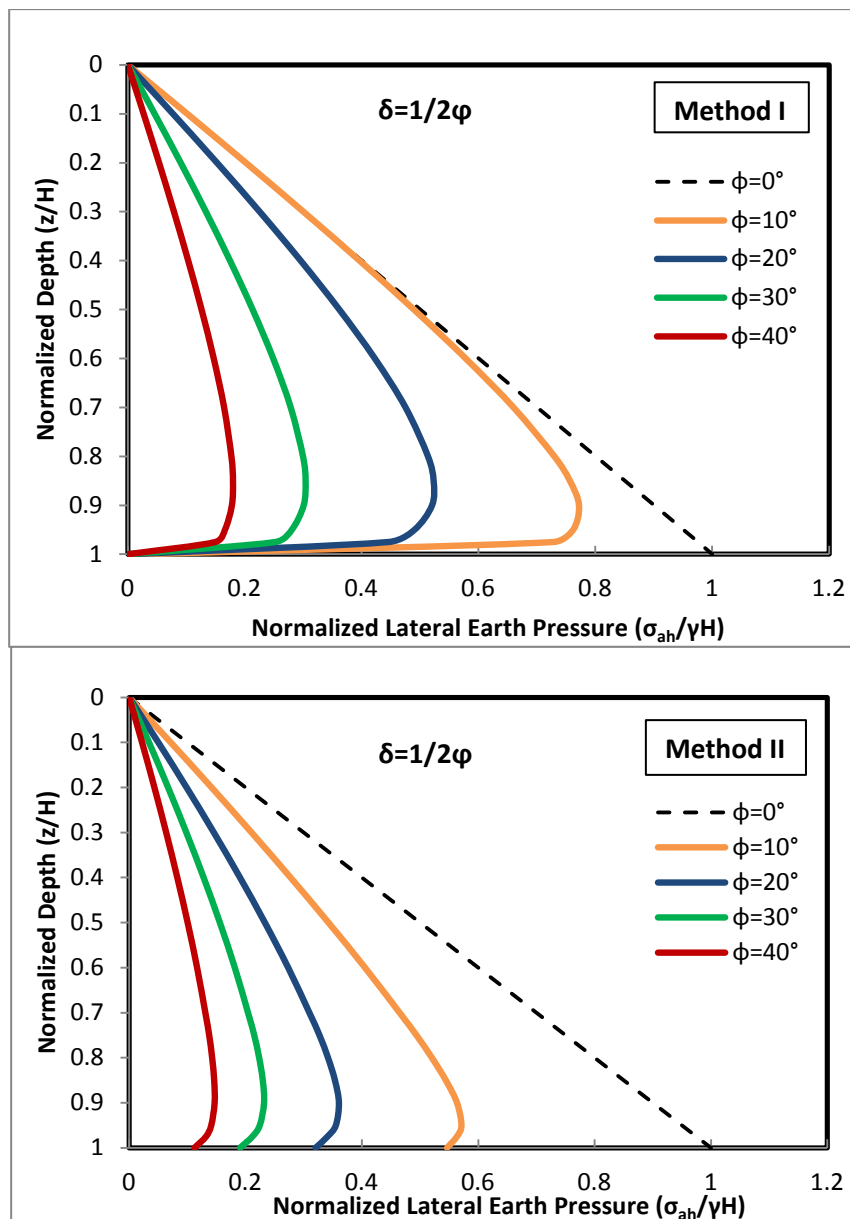


Figure 4-4 Lateral active earth pressure distributions obtained by Method I and Method II for various ϕ values

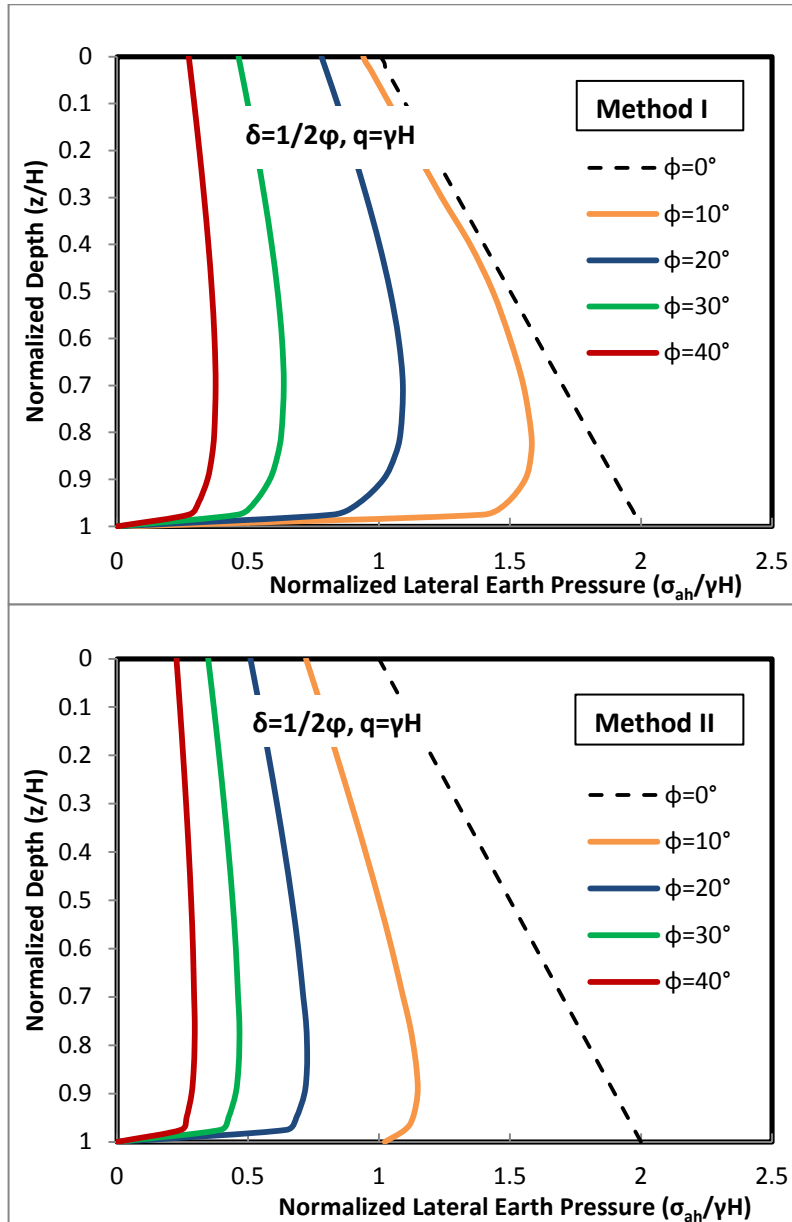


Figure 4-5 Lateral active earth pressure distributions under surcharge load of $q=\gamma H$ for various backfill internal friction angles (ϕ)

In Figure 4-5, normalized lateral earth pressures for the backfills with surcharge loads are presented. It is observed that surcharge has a more pronounced effect on the lateral earth pressures for the backfills having relatively small internal friction angles since lateral earth pressure ratio is dependent on the internal friction angle.

4.2.3 Effect of wall-backfill interface friction angle on lateral active earth pressures

The effect of soil – wall interface friction angle, δ on the distribution of the active earth pressures are presented in Figure 4-6 for a backfill material having internal friction angle of $\phi_{backfill}=40^\circ$. The distribution of the lateral active earth pressure is triangular for $\delta=0^\circ$ case, which is in agreement with Rankine’s lateral earth pressure theory. Active earth pressure distributions change from triangular to curvilinear shape as δ increases.

According to Figure 4-6, active earth pressures in the upper half of the retaining wall increases whereas a decrease occurs at the lower half of the wall as wall-backfill interface friction angle increases. As a result, the distance of the application point of the active earth thrust measured from the base of the wall increases with increasing interface friction angle. This consequence is also depicted in Figure 4-12. Method I gives higher lateral active earth pressures as compared to Method II for the same internal friction angle and soil-wall interface friction angle combinations as it can be inferred from the above two graphs. It is noted that predictions made by Method II are more realistic compared to Method I since pressures are in better agreement with actual data and non-zero lateral active earth pressures are observed at the base of the retaining wall.

Normalized lateral active earth pressures for different wall-backfill interface friction angle is compared for Method I and Method II including the effects of surcharge in Figure 4-7. It is observed that normalized lateral active earth pressures for both methods give linear distribution for zero wall-backfill internal friction angle, δ . This finding is consistent with earth pressure values predicted according to Rankine's theory. Nevertheless, as the wall-backfill interface friction angle gets closer to the internal friction angle of the soil, normalized lateral active earth pressure values become higher and the position of the peak lateral stress moves up towards the surface of the backfill for both methods. Method I predicts higher lateral active earth pressures as compared to Method II for the same wall-backfill interface friction angles as can be inferred from Figure 4-7. It should be addressed that results of the Method II are more realistic compared to Method I as Method II gives non-zero lateral active earth pressures at the base of the retaining wall.

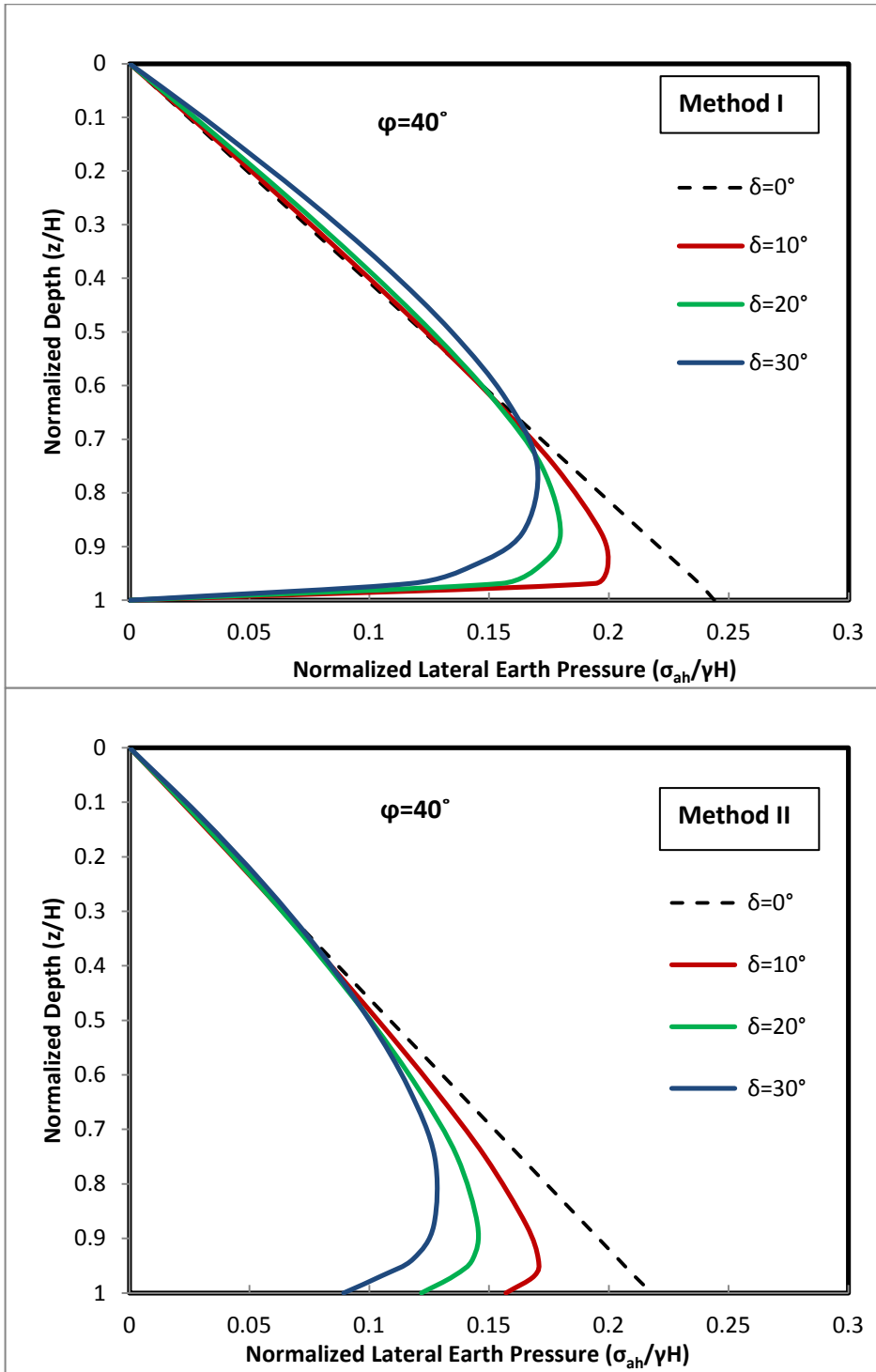


Figure 4-6 Lateral active earth pressure distribution for various wall-backfill interface friction angles (δ)

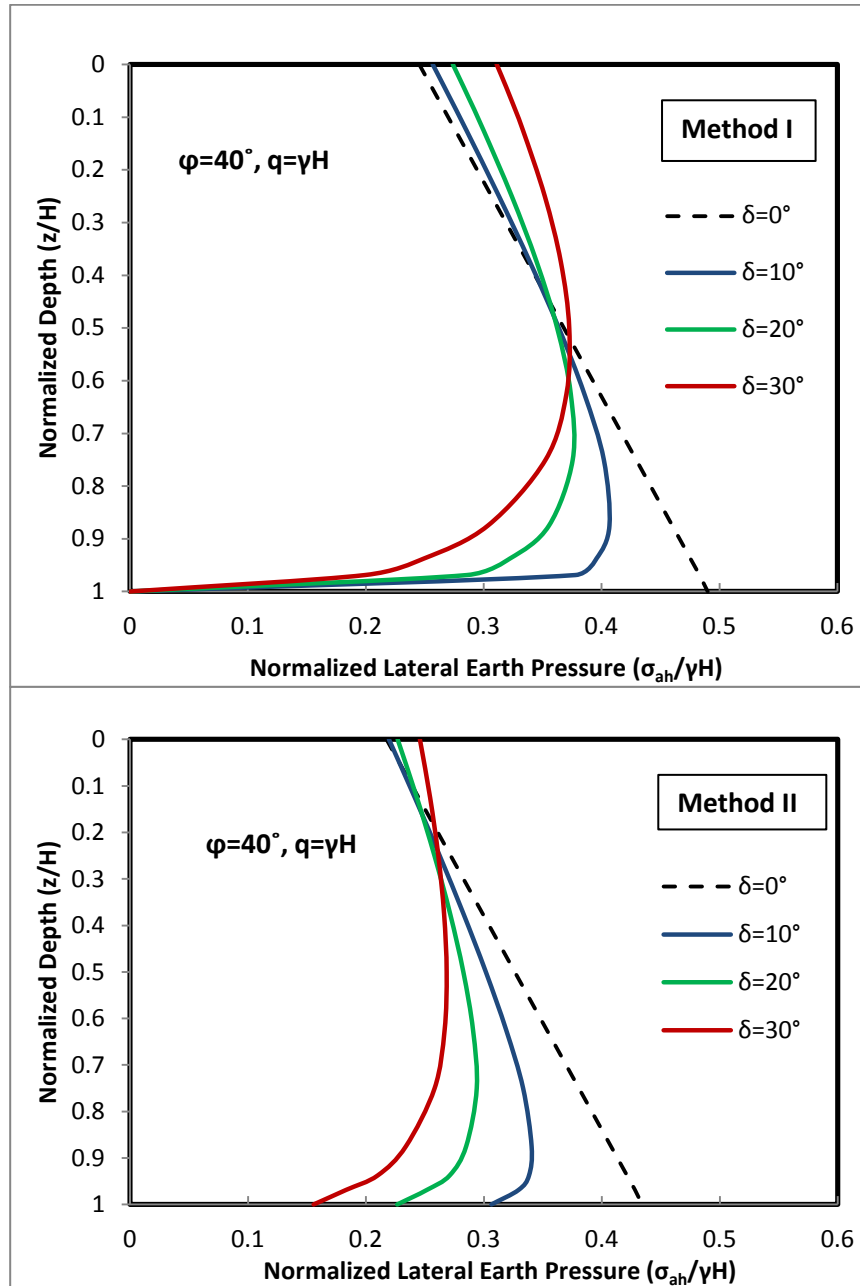


Figure 4-7 Lateral active earth pressure distributions under surcharge load of $q=\gamma H$ for various wall-backfill interface friction angles (δ)

4.2.4 Effect of retaining wall height on lateral active earth pressures

The lateral active earth pressure distributions for different retaining wall heights were depicted in Figure 4-8 for $\varphi = 3/4\delta = 30^\circ$. As it can be observed from the figure, the shapes of the distributions are the same for different retaining wall heights which means that the height of the retaining wall does not have an effect on the shape of the lateral active earth pressure distribution. In addition, as explained in the former results, Method I results in higher lateral active earth pressures compared to Method II and the results of

Method II are observed to be more realistic compared to Method I since Method II gives non-zero lateral active earth pressures at the base of the retaining wall.

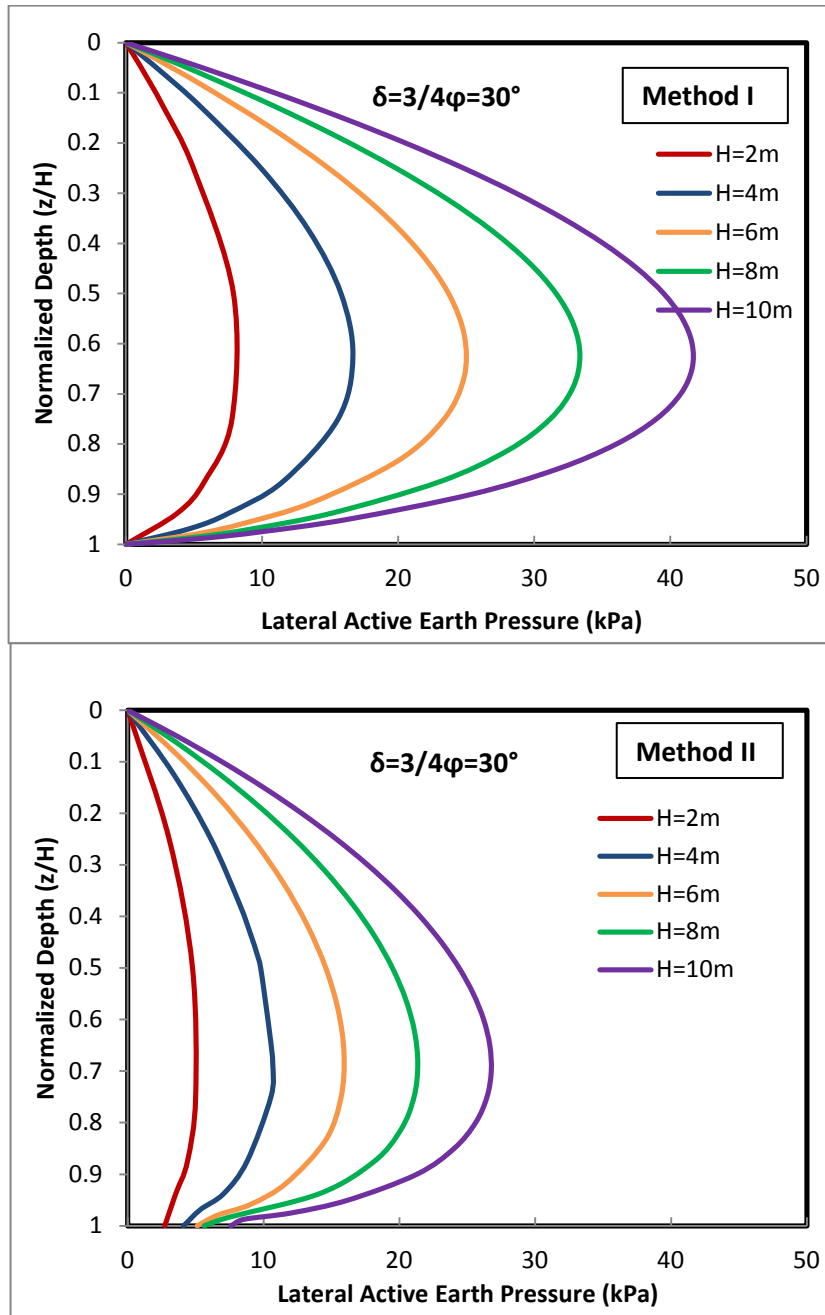


Figure 4-8 Effect of earth pressure distribution with the height of retaining wall

4.3 Comparison of Lateral Active Earth Thrust Calculated with Different Methods

The lateral earth forces are calculated by the numerical integration of the lateral pressure curves for different lateral earth pressure theories. Comparisons are made for the lateral active earth thrust normalized with the value calculated with Coulomb's theory. The effect

of internal friction angle and wall-backfill interface friction angle on total lateral active soil thrust are discussed in the following sections.

4.3.1 Comparison of lateral active earth thrust normalized with Coulomb's total lateral active earth thrust

Lateral active earth force is normalized by dividing the total active earth force predicted by different methods to the lateral load calculated with Coulomb's Theory. Results obtained by Coulomb (1776), Handy (1985), Wang (2000), Paik & Salgado (2003), Method I and Method II are presented in Table 4-1. Normalized lateral active earth thrusts ($P_{ah}/P_{ah,Coulomb}$) are indicated for a backfill internal friction angle of 40° and wall-backfill interface friction angle of $\delta = 2/3\phi = 27^\circ$.

Table 4-1 Total lateral active earth force normalized with Coulomb's total lateral earth thrust

METHOD	$P_{ah}/P_{ah,Coulomb}$
Coulomb (1776)	1
Handy (1985)	0.9
Wang (2000)	1
Paik & Salgado (2003)	1.11
Method I	1.29
Method II	0.94

It should be addressed that the results obtained with Method I are the highest whereas those calculated with Handy Method (1985) resulted in the lowest normalized lateral active earth thrust. Earth force predicted with Wang (2000) and Coulomb (1776) approaches give identical lateral active earth force values since these theories suggest similar formulations for the lateral earth thrust. Values estimated with Method II are lower than those of the Paik & Salgado (2003) approach since a parabolic critical failure line is taken into account for Method II while Paik and Salgado (2003) considers planar critical failure surface. It is observed that parabolic failure surface assumption leads to lower lateral load on the retaining wall.

4.3.2 Effect of internal friction angle on lateral active earth thrust

In Figure 4-9, the magnitude of lateral active earth thrust for different backfill internal friction angles are compared. It is observed that lateral active earth force exhibits a decreasing trend with increasing internal friction angle.

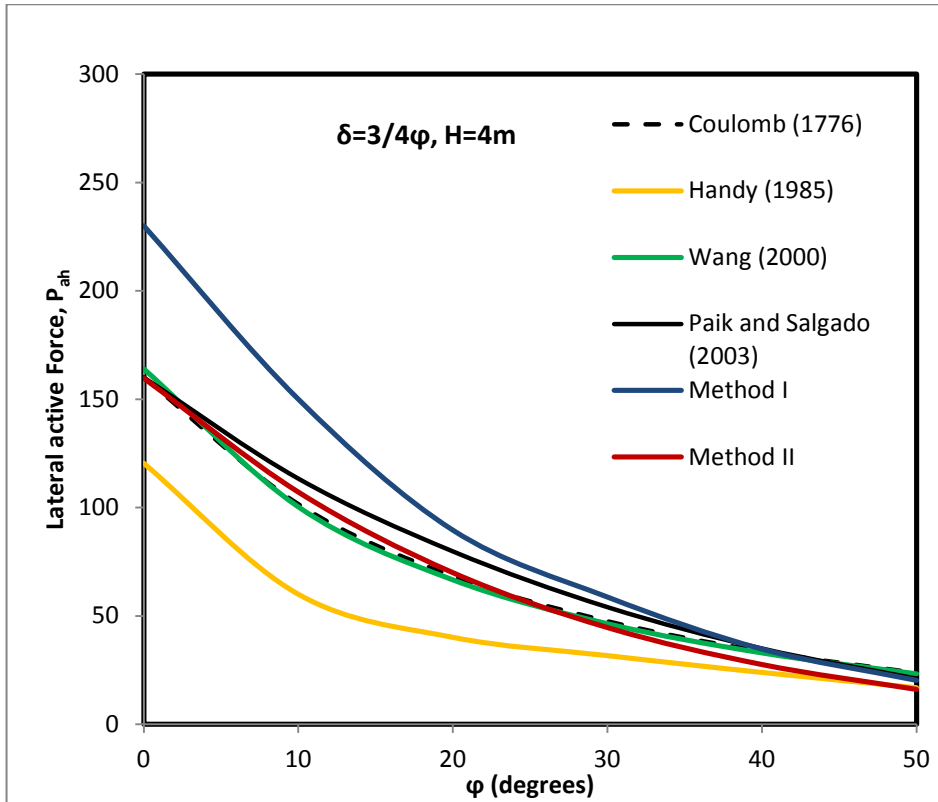


Figure 4-9 Effect of internal friction angle on lateral active force

Results of the Method II is found to be a lower bound and Method I is an upper bound for internal friction angles between $\varphi = 0^\circ$ to $\varphi = 30^\circ$. Beyond internal friction angles of $\varphi = 30^\circ$, all of the methods give nearly close results. These results are observed to be in conformity with the lateral active earth pressure distributions given in Figure 4-1 as Method I calculate relatively higher and Method II result in lower lateral active soil pressures. Besides, the resultant earth forces calculated by Wang (2000) theory are similar with those calculated by Coulomb's formula.

4.3.3 Effect of wall-backfill interface friction angle on lateral active earth thrust

Figure 4-10 shows the change of the lateral active force acting on a translating rigid retaining wall having various wall-backfill interface friction angles (δ) between 0° and 30° for a constant internal friction angle $\varphi = 40^\circ$. In the same figure, results obtained by Coulomb (1776), Handy (1985), Wang (2000) and Paik and Salgado (2003) are presented together with the predictions of Methods I and II. According to Figure 4-10, Method I gives the highest lateral active earth force. As the wall-backfill interface friction angle approaches to the internal friction angle of the soil, Method I provide even higher results. It is figured out that the results obtained by Handy and Method II resulted in approximately similar results for wall-backfill interface friction angles of less than 15° . Beyond this value, Method II gives the lowest values with a minimum of approximately 30° .

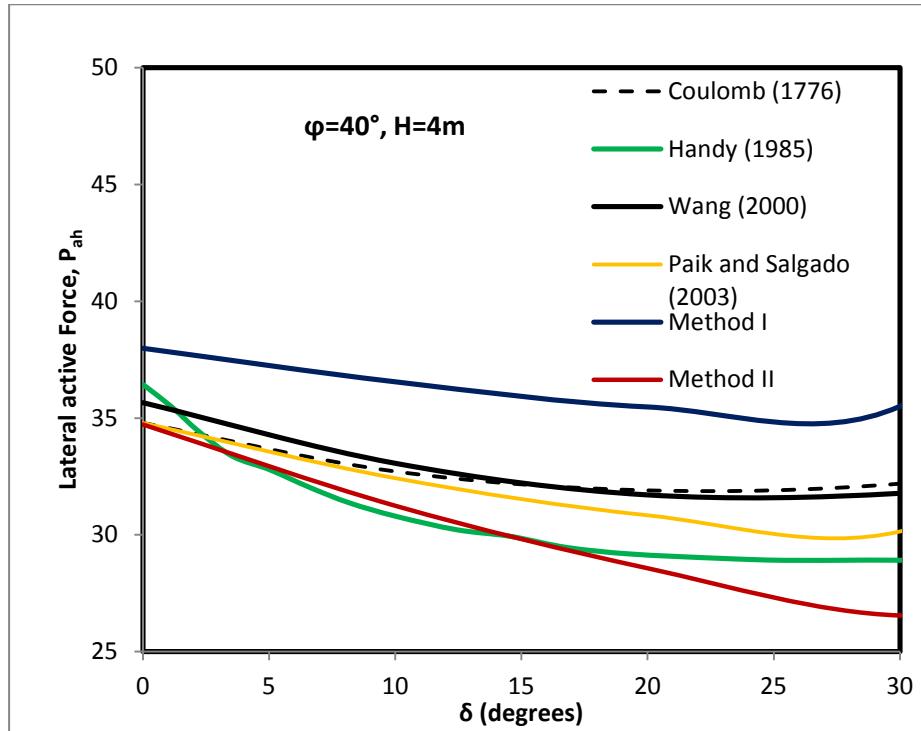


Figure 4-10 Effect of wall-backfill interface friction angle on lateral active earth force

4.4 Application Point of the Total Lateral Active Thrust

The resultant lateral active soil pressures and the location of their application are calculated numerically by integrating the earth pressure curves. Point of application of lateral active earth thrust are estimated with different methods and values are compared and the effect of internal friction angle and wall-backfill interface friction angle on the point of application of lateral active force are discussed in the following sections.

4.4.1 Height of application point of lateral active earth force normalized with wall height

Table 4-2 indicates the point of application of lateral active earth thrust predicted by different methods normalized with wall height. In this table, lateral earth force calculated with Coulomb (1776), Handy (1985), Wang (2000) and Paik & Salgado (2003) approaches are illustrated together with the predictions made by Methods I and II.

Table 4-2 Height of application point of lateral active earth force normalized with wall height

METHOD	h/H
Coulomb (1776)	0.33
Handy (1985)	0.48
Wang (2000)	0.39
Paik & Salgado (2003)	0.42
Method I	0.44
Method II	0.42

Application point of the lateral active force is estimated as 0.42H according to Paik & Salgado approach (2003) and proposed Method II. On the other hand, both methods provide different lateral active earth thrust results as illustrated in Table 4-1. Based on observations related with Table 4-2, it can be said that application point estimated with Method I is higher compared to those predicted by Paik & Salgado (2003) and Method II, whereas application point given by Handy's solution (1985) provides the highest application point. Coulomb's theory does not provide the distribution of lateral stresses along the wall height; however, it is generally assumed that a triangular distribution occurs and application point is located at 0.33H above the wall base for Coulomb's approach. Normalized height of application point of lateral active earth force predicted by different methods except for the one made by Wang (2000) are consistent with the finding made by Handy (1985) that for a rigid translating retaining wall, the height of the application point of lateral active earth force varies between 0.4 and 0.5 times the wall height. Since the non-linearity of the stress profile increases with soil arching effect, application point of the total active thrust rises up to approximately 0.43H which is 30% higher than the mostly used value of 0.33H.

4.4.2 Effect of internal friction angle on the point of application of lateral active force

In Figure 4-11, point of application of lateral active earth thrust from the base of the wall for different internal friction angle of backfill calculated with different approaches are presented. Elevation of the application points are normalized by dividing the values to the total height of the wall.

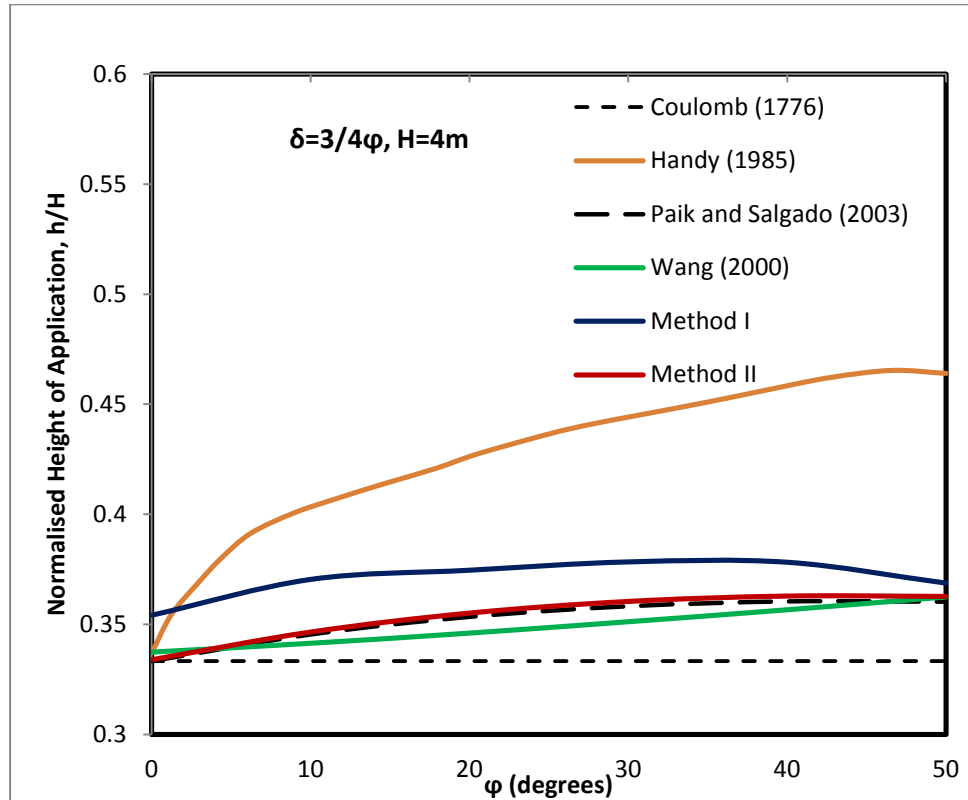


Figure 4-11 Effect of backfill internal friction angle on normalized height of application of lateral active earth force

According to the approaches incorporating lateral arching theory, application point of active thrust rises as internal friction angle of the backfill increases. This behavior is observed for all of the investigated approaches except for Coulomb's earth pressure theory. Since the shape of the pressure profiles becomes significantly nonlinear as the effect of lateral arching increases, the pressures within the upper portion of the retaining wall becomes higher and consequently elevation of the application points rises. It is observed that the Handy's solution (1985) resulted in relatively higher height of application when compared to the other methods. Besides, Paik & Salgado (2003) and Method II provide similar results for the height of application point for the same internal friction angles. However, Method I results in relatively higher normalized height of application of lateral active earth forces compared to results of Wang (2000), Paik & Salgado (2003) theories and Method II.

4.4.3 Effect of wall-backfill interface friction angle on the point of application of lateral active force

Point of application of the lateral active force for different wall-backfill friction angle values are calculated with several methods. In Figure 4-12, normalized application points (h/H) are indicated for a retaining wall with height of 4 meters and backfill internal friction angle of 40° . It is observed that methods incorporating arching theory provide higher values for the location of the application point since these methods predict higher earth pressure values within the upper half of the retaining wall height.

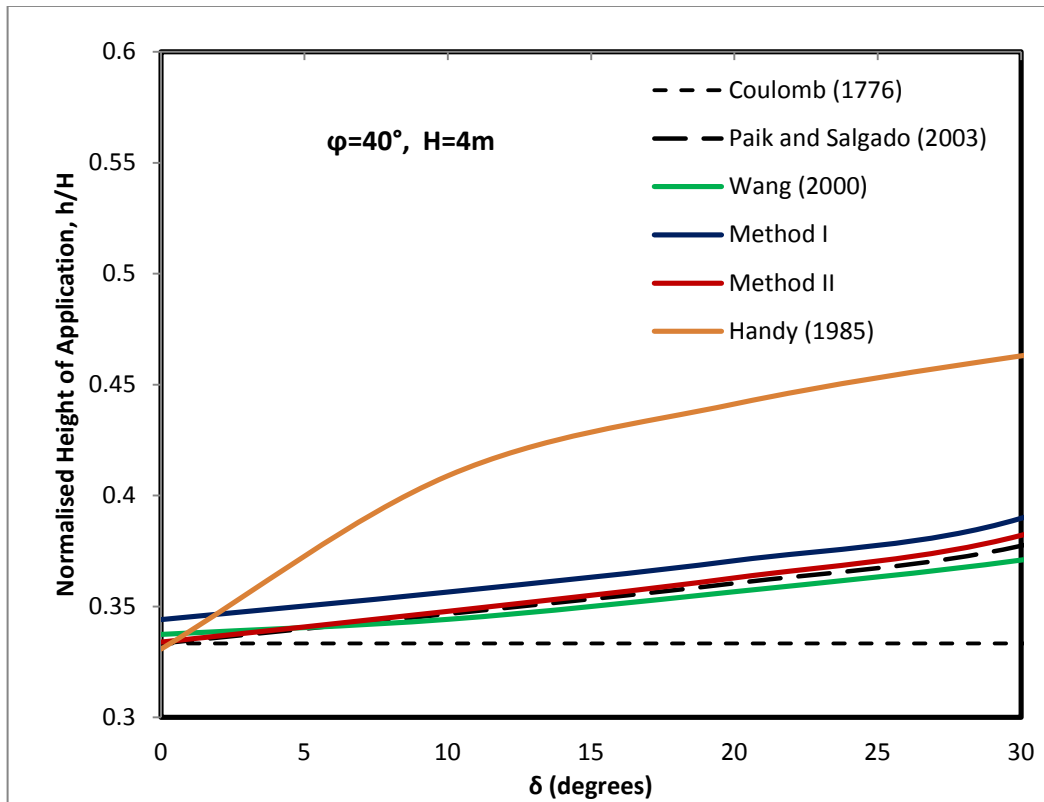


Figure 4-12 Effect of δ on the height of application of lateral active earth force

Handy's solution (1985) yields relatively higher predictions for the application point compared to the other methods since the shape of the pressure profile is significantly different from those observed in the other approaches. This condition results from the shortcomings in the K_w formulation given in Equation (2-9). Additionally, Paik & Salgado (2003) and Method II give similar values for the same internal friction angles. Nevertheless, Method I yields relatively higher values compared to Wang (2000), Paik & Salgado (2003) and proposed Method II.

4.5 Comparison of Lateral Earth Pressure Coefficients Calculated with the Suggested Formulations

Lateral earth pressure coefficients calculated with Methods I and II are compared in Figure 4-13. In order to simplify the use of these equations given in Equation (3-18) and Equation (2-13), design charts for lateral active earth pressure coefficients for different ϕ and δ combinations are given in this figure. Predictions are compared to those calculated with Rankine's and Coulomb's theories. Method I over predicts lateral stresses since K_{ap} which is defined as the active lateral earth pressure ratio for parabolic concave arch given in Equation (3-18), provides relatively high active lateral stress ratios. On the other hand, both Method I and Method II provide more satisfactory values compared to Rankine's and Coulomb's theory since the proposed methods take into the account the effect of arching through the lower part of the retaining wall. According to the estimations made with Method I and II, lateral earth pressure coefficients slightly increase as the friction between the wall-backfill increases. This increase is associated with the decrease of the rotation

angle between horizontal and σ_1 (Figure 3-5) which increases the horizontal component of the lateral earth load acting on the rigid wall.

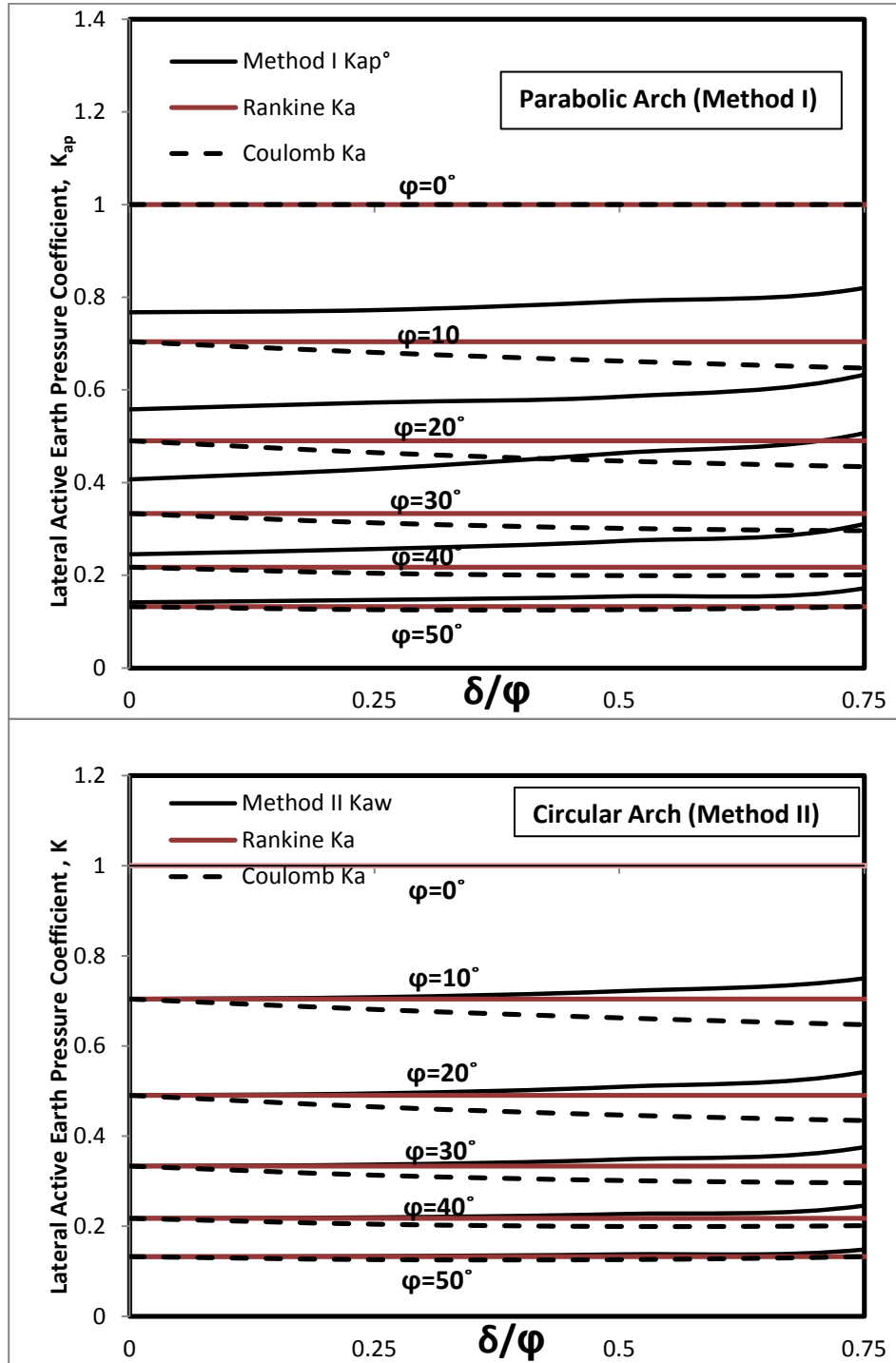


Figure 4-13 Effect of ϕ and δ lateral active earth pressure coefficients for granular soils

CHAPTER 5

SUMMARY AND CONCLUSIONS

5.1 Summary

Estimation of the active lateral earth pressures is very important in the design of earth retaining walls. Civil engineers have traditionally calculated the active earth pressure against rigid retaining walls using either Coulomb's or Rankine's theories. Generally it is assumed that the distribution of active earth pressure acting upon the retaining wall is linear; however, experimental results (Tsagareli, 1965 and Fang & Ishibashi, 1986) indicate that the distribution of active earth pressure behind a rough rigid wall is nonlinear. The nonlinearity of the active earth pressure distribution results from arching effects that were expressed by Handy in 1985.

Within the scope of this thesis study, new analytical formulations are suggested to estimate the lateral active earth pressures acting on rigid retaining walls translating away from the backfill. Within the first formulation, shape of the failure surface is taken as linear whereas a parabolic concave soil arch was considered to obtain lateral pressure distributions. In the second formulation, a curvilinear failure surface is considered with a circular soil arch segment between the retaining wall and the failure surface. The lateral pressure distribution relationships are formulated according to these assumptions and two different formulations are suggested for the estimation of lateral soil pressures considering soil arching effects. As the last contribution, lateral active earth pressure expression suggested by Paik and Salgado (2003) is extended to include surcharge effects on the lateral earth pressures. Lateral pressure distributions estimated by the proposed methodologies are validated against physical test data and compared with the predictions of previous earth pressure theories. Proposed analytical models are further calibrated for a better fit with the actual test data near the wall base. Subsequently, a parametric study is performed to investigate the influence of backfill friction angle, wall height and wall-backfill interface friction angle on the lateral earth pressure distribution, total active thrust and application point of the active force. Lateral soil pressures behind rigid translating retaining wall, including surcharge load effects, are calculated from different methods and compared for a normalized surcharge value of $q = \gamma H$.

5.2 Research Findings

Within the framework of the parametric study based on the analytical formulations suggested in the literature and within this thesis, following conclusions are made:

Lateral active earth pressure distribution acting on a yielding rigid retaining wall is found to be curvilinear when lateral soil arching effects were taken into account. Predictions made with Method I and Handy's solution (1985) yields the highest lateral earth pressures between 70% and 90% of the wall height, respectively. Method II formulations provide the best approximation of the actual test data.

Method I over predicts lateral stresses since K_{ap} which is defined as the active lateral earth pressure ratio for parabolic concave arch provides relatively high active lateral stress ratios compared to Method II. Although the critical failure planes make an angle of $\alpha = 45^\circ + \varphi/2$ with the horizontal at the base of the retaining wall height for both approaches, Method II predicts lower horizontal stress values since a parabolic critical failure surface is assumed in this approach. Shape of the failure surface affects the amount of mobilized soil shear strength and also the weight of the active soil wedge. On the other hand, both Method I and Method II provide more satisfactory values compared to Coulomb's theory since the proposed methods take into the account the effect of arching through the lower part of the retaining wall.

Surcharge induced earth pressure distributions obtained with Method II constitute a lower bound for Wang and modified Paik-Salgado approaches whereas predictions of Method I give an upper bound. Although Method II and Modified Paik and Salgado approach give the same lateral normalized stress ratios at the wall top, Method II estimates lower stress ratios along the wall height since it considers the shape of the critical failure line as parabolic whereas modified Paik and Salgado approach assumes a planar failure surface.

Additionally, surcharge induced lateral earth pressure distribution proposed by Wang (2000) exhibits a different geometry compared to the other approaches. This is due to the fact that Wang does not take a suitable lateral earth pressure coefficient into account, although the lateral earth pressure coefficient has a significant effect on the distribution of the lateral earth pressures as explained by Paik and Salgado (2003). A closed form solution for the lateral earth pressure coefficient was not suggested by the author. The analyses are carried out by making assumptions for K values.

The distribution of the active earth pressure with and without surcharge become more non-linear as the internal friction angle of the soil increases from $\varphi = 0^\circ$ to $\varphi = 40^\circ$. It is also observed that the active earth pressure behind the rigid translating retaining wall decreases as the internal friction angle of the soil increases. Method I gives higher lateral active earth pressures compared to Method II for the same internal friction angle. Besides, Method II gives non-zero pressure values at the base of the retaining wall which exhibits a better agreement with the physical test results carried out by Fang and Ishibashi (1986).

It is observed that normalized lateral active earth pressures with and without surcharge load, for both methods, have linear distribution for zero wall-backfill internal friction angle, δ . This finding is consistent with earth pressure values predicted according to Rankine's theory. Nevertheless, as the wall-backfill interface friction angle gets closer to the internal friction angle of the soil, normalized lateral active earth pressure values become higher and the position of the peak lateral stress move up towards the surface of the backfill for both methods. Method I predicts higher lateral active earth pressures as compared to Method II for the same wall-backfill interface friction angles. It should be

addressed that results of the Method II are more realistic compared to Method I as Method II gives non-zero lateral active earth pressures at the base of the retaining wall.

According to the results of the parametric analyses, lateral earth forces obtained with Method I are the highest whereas those calculated with Handy Method (1985) are the lowest lateral active earth thrust normalized with respect to Coulomb's theory. Wang (2000) and Coulomb (1776) approaches yield identical lateral active earth force values since lateral earth thrust formulations are similar in these theories. Values estimated with Method II are lower than those of the Paik and Salgado approach since a parabolic critical failure line is taken into account for Method II while Paik and Salgado (2003) considers planar critical failure surface. It is observed that parabolic failure surface assumption leads to lower lateral load on the retaining wall.

It is observed that lateral active earth force exhibits a decreasing trend with increasing internal friction angle. Results of the Method II are found to be a lower bound and Method I provides an upper bound for internal friction angles between $\varphi = 0^\circ$ to $\varphi = 30^\circ$. Beyond internal friction angles of $\varphi = 30^\circ$, all of the methods give close results.

Application point of the lateral active force is estimated as 0.42H according to Paik & Salgado approach (2003) and proposed Method II. On the other hand, both methods provide different lateral active earth thrust results. It can be said that application point estimated with Method I is higher compared to those predicted with Paik & Salgado (2003) and Method II, whereas application point given by Handy's solution (1985) provides the highest application point. Coulomb's theory does not provide the distribution of lateral stresses along the wall height; however, it is generally assumed that a triangular distribution occurs and application point is located at 0.33H above the wall base for Coulomb's approach. Normalized height of application point of lateral active earth force predicted by different methods except for the one made by Wang (2000) are consistent with the finding made by Handy (1985) that the height of the application point of lateral active earth force varies between 0.4 and 0.5 times the wall height. Since the non-linearity of the stress profile increases with soil arching effect, application point of the total active thrust rises up to approximately 0.43H which is 30% higher than the mostly used value of 0.33H.

5.3 Conclusions

According to the approaches incorporating lateral arching theory, application point of active thrust rises as internal friction angle of the backfill increases. This behavior is observed for all of the investigated approaches except for Coulomb's earth pressure theory. Since the shape of the pressure profiles becomes significantly nonlinear as the effect of lateral arching increases, the pressures within the lower portion of the retaining wall becomes smaller and consequently point of application of the resultant lateral force rises.

In order to simplify the use of lateral earth pressure coefficients calculated with Methods I and II, design charts for lateral active earth pressure coefficients for different φ and δ combinations are presented. Values calculated with the suggested methodologies are compared to those of Rankine's and Coulomb's theories. Method I over predicts lateral

stresses since K_{ap} which is defined as the active lateral earth pressure ratio for parabolic concave arch is greater in this case. On the other hand, both of Methods I and II provide more satisfactory values compared to Rankine's and Coulomb's Theories since the suggested formulations take into the account the effect of arching through the lower part of the retaining wall. According to the estimations made with Methods I and II, lateral earth pressure coefficients for total active force calculations slightly increase as the friction between the wall and backfill increases. This increase is associated with the decrease of the rotation angle between horizontal and σ_1 (Figure 3-5) which increases the horizontal component of the lateral earth load acting on the rigid wall.

Lateral soil arching induced within the granular material has a significant influence on the lateral pressure distribution acting on rigid and yielding walls. The non-linearity of the pressure profile becomes more dominant as wall-backfill interface friction increases. According to the parametric analyses performed with the suggested methodologies, lateral earth thrust acting on yielding rigid walls significantly decreases as wall-backfill interface friction angle increases. Although Coulomb's Theory takes the interface friction force into account in the equilibrium of the forces acting on the active soil wedge, it does not fully represent the influence of lateral soil arching. The formulations suggested within this study may serve as a useful starting point for developing advanced methodologies to make more realistic representation of the actual behavior.

5.4 Recommendations for Future Work

As a future work, the formulations may be extended to include not only rigid walls but also flexible retaining walls such as cantilever walls and mechanically stabilized earth walls. Different types of wall movements such as rotation about top or bottom as well as translation can be considered in the development of the future formulations. The horizontal slice method that is suggested in this study can be further developed to obtain a more practical and versatile formulation for lateral earth pressures. To make a more extensive validation of the formulations presented within this thesis study, the results obtained by Method I and Method II should be compared with those of field measurements and physical tests performed for translating rigid walls retaining granular soils.

REFERENCES

1. American Association of State Highway and Transportation Officials. (1987) Task Force 27. Guidelines for the Design of Mechanically Stabilized Earth Walls. Draft version. Washington.
2. Chevalier, B., Combe, G. & Villard, P. (2008). Experimental and Numerical Studies of Load Transfers and Arching Effect. The 12th International Conference of International Association for Computer Methods and Advances in Geomechanics (IACMAG) October, 1-6, 2008, Goa, India, from: <http://www.civil.iitb.ac.in/~dns/IACMAG08/pdfs/A35.pdf>, last access date 12.04.2013
3. Coulomb, C. A. (1776). Essai sur une application des re`gles des maximis et minimis a` quelques proble`mes de statique relatifs a` l'architecture. Me`m. Acad. Roy. Pre`s. Divers Savants 7, Paris.
4. Costa, Y. D., Zornberg, J. G., Bueno, B. S., & Costa, C. L. (2009). Failure Mechanisms in Sand over a Deep Active Trapdoor. *Journal of Geotechnical and Geoenvironmental Engineering*, 135(11), 1741-1753. doi: Doi 10.1061/(Asce)Gt.1943-5606.0000134
5. Craig, R. F., (1997). *Soil mechanics*. London and New York: Spon Press.
6. Gazetas, Gazetas, G., Psarropoulos, P. N., Anastasopoulos, I., & Gerolymos, N. (2004). Seismic behavior of flexible retaining walls subjected to short duration moderately strong excitation. *Soil Dynamics and Earthquake Engineering*, 24, 537-550.
7. Deb, K. (2010). A mathematical model to study the soil arching effect in stone column-supported embankment resting on soft foundation soil. *Applied Mathematical Modelling*, 34(12), 3871-3883. doi: DOI 10.1016/j.apm.2010.03.026
8. Fang, Y. S., & Ishibashi, I. (1986). Static Earth Pressures with Various Wall Movements. *Journal of Geotechnical Engineering-Asce*, 112(3), 317-333.
9. Handy, R. L. (1973). Igloo and Natural Bridge as Ultimate Structures. *Arctic*, 26(4), 276-281.
10. Handy, R. L. (1985). The Arch in Soil Arching. *Journal of Geotechnical Engineering-Asce*, 111(3), 302-318.
11. Jaky, J. (1944). The coefficient of earth pressure at rest. *J. Soc. Hungarian Architect and Engineering*, 7. 355-358.

12. Janssen, H. A. (1895). Versuche über getreidedruck in silozellen. Zeitschrift, Verein Deutscher Ingenieure 39, 1045–1049 (partial English translation in Proc. Inst. Civ. Engrs, 1986, 553.
13. Krynine, D. P. (1945). Discussion of “Stability and stiffness of cellular cofferdams.” by K. Terzaghi.” ASCE Trans., 110, 1175–1178.
14. Lambe, T. W. & Whitman, R. V. (1969). Soil Mechanics. John Wiley and Sons.
15. Livingston, C. W. (1961). The natural arch, the fracture pattern, and the sequence of failure in massive rock surrounding an underground opening. Proceedings of the symposium on rock mechanics, Pennsylvania State University, Bulletin 76, 197-201.
16. Marston, A. (1930). “The theory of external loads on closed conduits in the light of latest experiments.” Bulletin No. 96, Iowa Engineering Experiment Station, Ames, Iowa.
17. Nadukuru, S. S., & Michalowski, R. L. (2012). Arching in Distribution of Active Load on Retaining Walls. Journal of Geotechnical and Geoenvironmental Engineering, 138(5), 575-584. doi: Doi 10.1061/(Asce)Gt.1943-5606.0000617
18. Paik, K. H., & Salgado, R. (2003). Estimation of active earth pressure against rigid retaining walls considering arching effects. Geotechnique, 53(7), 643-653. doi: DOI 10.1680/geot.53.7.643.37385
19. Terzaghi, K. (1943). Theoretical soil mechanics. New York: Wiley.
20. Tsagareli, Z. V. (1965). Experimental investigation of the pressure of a loose medium on retaining walls with a vertical back face and horizontal backfill surface. J. Soil Mech. Found. Engng, ASCE 91, No. 4, 197–200.
21. Rankine, W. J. M. (1857). On the stability of loose earth. Philos. Trans. R. Soc. London, 147, 9–27.
22. Spangler, M. G., & Handy, R. L. (1984). Soil Engineering, Harper & Row, New York.
23. Walker, D. M. (1966). An Approximate Theory for Pressures and Arching in Hoppers. Chemical Engineering Science, 21(11), 975-&. doi: Doi 10.1016/0009-2509(66)85095-9
24. Wang, Y. Z. (2000). Distribution of earth pressure on a retaining wall. Geotechnique, 50(1), 83-88.

APPENDIX A

DERIVATIONS

A.1 Determination of the Rotation Angle

In order to obtain Equation (3-13) assume that $x = \tan \theta$ whose formulation is given in Equation (3-12),

$$x = \frac{N + x^2}{N - 1} \tan \delta \quad (7-1)$$

That is equal to,

$$Nx - x = N \tan \delta + x^2 \tan \delta \quad (7-2)$$

Both sides are divided by $\tan \delta$ in Equation (7-2),

$$x^2 + x \left(\frac{-N + 1}{\tan \delta} \right) + N = 0 \quad (7-3)$$

that yields the second order equation. The roots of this second order equation can be obtained as,

$$x_1, x_2 = \frac{\frac{N - 1}{\tan \delta} \pm \sqrt{\left(\frac{N - 1}{\tan \delta}\right)^2 - 4N}}{2} \quad (7-4)$$

when the $x = \tan \theta$ expression is replaced in Equation (7-4), $\tan \theta$ can be obtained as follows,

$$\tan \theta = \frac{(N - 1) \pm \sqrt{(N - 1)^2 - 4N \tan^2 \delta}}{2 \tan \delta} \quad (7-5)$$

which results in Equation (3-13).

A.2 Determination of Rate of Change of Failure Angle

The rate of change of failure angle which is represented by α is obtained by using trigonometric relationships. Figure 7-1 indicates the failure angle α formed within a slice at the failure zone. From this figure, the α angle can be expressed as,

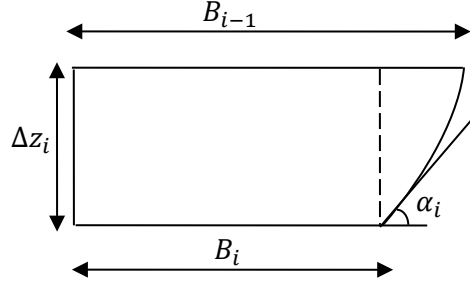


Figure 7-1 A slice showing the failure angle within the failure zone at the back of the retaining wall

$$\tan\left(\frac{\pi}{2} - \alpha\right) = \frac{(B_{i-1}) - (B_i)}{\Delta z_i} \quad (7-6)$$

and the upper and lower widths of the slice is expressed by using the roots of second order equation of the failure surface formulation given in Equation (3-26) including a, b and c constants,

$$B_i = \frac{-b \pm \sqrt{b^2 - 4a(c-z_i)}}{2a} \text{ and } B_{i-1} = \frac{-b \pm \sqrt{b^2 - 4a(c-z_{i-1})}}{2a} \quad (7-7)$$

these B_i and B_{i-1} expressions are placed into Equation (7-6) and finally Equation (3-27) can be obtained.

A.3 Determination of Paik and Salgado Lateral Soil Arching (2003) Approach to Include Surcharge Effect

Assume that the expression given in Equation (3-1) $K_{aw} \tan \delta \tan \theta$ is represented by A for simplicity, then Equation (3-1) becomes,

$$\left[\bar{\sigma}_v + \frac{\gamma}{1-A} (H-z) \right] (H-z)^{-A} = C \quad (7-8)$$

when the boundary conditions of $\bar{\sigma}_v = q$ at $z = 0$ are placed into the equation given above,

$$\left[q + \frac{\gamma(H-z)}{1-A} \right] H^{-A} = C \quad (7-9)$$

then the integral constant C is determined as,

$$C = \frac{\gamma H}{(1-A)H^A} + \frac{q}{H^A} \quad (7-10)$$

The general equation given in Equation (7-6) is equated to the integral constant given above,

$$\left[\bar{\sigma}_v + \frac{\gamma}{1-A} (H-z) \right] (H-z)^{-A} = \frac{\gamma H}{(1-A)H^A} + \frac{q}{H^A} \quad (7-11)$$

which yields,

$$\bar{\sigma}_v = \left[\frac{\gamma H (H-z)^A}{(1-A)H^A} \right] + \frac{q(H-z)^A}{H^A} - \frac{\gamma(H-z)}{(1-A)} \quad (7-12)$$

when the expression $A = K_{aw} \tan \delta \tan \theta$ replaced into Equation (7-10), the following formula is obtained as,

$$\bar{\sigma}_v = \left(\frac{\gamma H}{1-K_{aw} \tan \delta \tan \theta} \right) \left[\left(1 - \frac{z}{H} \right)^{K_{aw} \tan \delta \tan \theta} - \left(1 - \frac{z}{H} \right) \right] + \left[q K_{aw} \left(1 - \frac{z}{H} \right)^{K_{aw} \tan \delta \tan \theta} \right] \quad (7-13)$$

lastly, substituting $\sigma_{ahw} = \bar{\sigma}_v K_{aw}$ into Equation (7-11) results in Equation (3-29).